AD NUMBER
AD848715
LIMITATION CHANGES

TO:

Approved for public release; distribution is unlimited.

FROM:

Distribution authorized to U.S. Gov't. agencies and their contractors; Critical Technology; DEC 1968. Other requests shall be referred to Air Force Aero Propulsion Laboratory, Attn AFSC, Wright-Patterson AFB, OH 45433. This document contains export-controlled technical data.

AUTHORITY

AFAPL ltr, 12 Apr 1972

AFAPL-TR-68-138

TWO-TERMINAL CONNECTED MHD GENERATORS
WITH LIQUID AND SOLID FUELS

John B. Dicks, Jr., Ying-chu Lin Wu, Dieter L.
Denzel, Siegbert Witkowski, Patricia Chang,
J W. Muehlhauser, Richard V. Shanklin, III,
Uwe Zitzow, Robert E Taylor and Edward S. Jett

The University of Tennessee Space Institute
Tullahoma, Tennessee

AFAPL-TR-68-138

TWO-TERMINAL CONNECTED MHD GENERATORS
WITH LIQUID AND SOLID FUELS

John B. Dicks, Jr., Ying-chu Lin Wu, Dieter L.
Denzel, Siegbert Witkowski, Patricia Chang,
J W. Muehlhauser, Richard V. Shanklin, III,
Uwe Zitzow, Robert E Taylor and Edward S. Jett

The University of Tennessee Space Institute
Tullahoma, Tennessee

NOTICES

FOREWORD

The MHD generator program was conducted under Contract AF 33(615)-2691, managed from the Air Force Aero Propulsion Laboratory (AFAPL), Project No. 5350, Task No. 535004, Air Force Systems Command (AFSC), Wright-Patterson Air Force Base, Ohio.

The University of Tennessee Space Institute was responsible for the design and construction of MHD generator channels, magnet and load bank, and directed the test program.

The tests were performed by ARO, Inc., contract operator of the Arnold Engineering Development Center (AEDC), AFSC, by personnel of the Rocket Test Facility. The test programs are reported in AEDC-TR-66-240, Experimental Performance of Two Segmented Wall Magnetohydrodynamic Electric Power Generators, R. J. LeBoeuf and M. A. Nelius, ARO, Inc., January 1967; AEDC-TR-67-174, Experimental Performance of a 60-Deg-Slant, Segmented Wall, Magnetohydrodynamic Electric Power Generator, R. J. LeBoeuf and J. D. McNeese, ARO, Inc., October 1967; and AEDC-TR-67-250, Experimental Performance of a Hall Magnetohydrodynamic Electric Power Generator, R. J. LeBoeuf and J. D. McNeese, ARO, Inc., December, 1967.

The solid fuel motors were supplied to us by Hercules Corporation.

This report was submitted by the authors: John B. Dicks, Jr., Ying-chu Lin Wu, Dieter L. Denzel, Siegbert Witkowski, Pat Chang, Joel Muehlhauser, Richard V. Shanklin, III, Uwe Zitzow, Robert E. Taylor and Edward S. Jett.

ii

ABSTRACT

Three DCW generators with side wall angles of 45°, 60° and 90° (Hall) of the same physical dimensions are studied. Two different types of fuels are used to drive the generator, liquid fuel consisting of RP1, gaseous oxygen and potassium hydroxide dissolved in alcohol, and double based solid fuel (manufactured and supplied by Hercules) with heavy potassium loading.

The solid fuel produced a very high conductivity (40-50 mhos/m) as compared to the liquid fuel, consequently the solid fuel generator out-performs the liquid fuel generator by a significant amount except for the Hall generator. With solid fuel the generated electrical power of a 45° DCW channel exceeded 200 KW during part of one test.

Another significant discovery of the solid fuel experiment is that the generators can run with aluminum oxide and potassium coating without large degradation in power output. Therefore, the deposit of solid particles may be used to increase generator lifetime by preventing electrode deterioration.

More refined theoretical work is carried out to include the finite segmentation effects and current-dependent electrode drop.

iii

TABLE OF CONTENTS

LIST OF FIGURES

NOMENCLATURE

A	Channel cross-sectional area
a/d	$\tan \theta$
B	Magnetic field strength
$\vec{B}$	Magnetic induction vector
b	Channel width
c	Normalized electrode length
c'	Normalized isolator length
C_p	Specific heat mixture
d	Channel height
dQ	Heat transfer per infinitesimal volume element
dR	External load
dX	Frictional force along channel
$\vec{E}$	Electric field intensity
e	Electron charge
e_i	Input signal to the amplifier at station i
H	Stagnation enthalpy
h	Specific enthalpy of gas mixture
h_i^o	Heat of formation of ith species
I	Total current
I_e	Electrode current
$\vec{j}$	Current density
L	Channel length
M	Mach number
$\dot{m}$	Mass flow rate
p	Pressure
R	Gas constant

R_{12} Time-averaged cross-correlation function

R_c Total resistance

r Scalar external resistivity

S_{12} Input cross-power spectrum density

S'_{12} Output cross-power spectrum density

T Temperature

t Time

$\tan \epsilon$ Generator operation parameter

u Gas velocity in x direction

u_1, u_2 Functions appeared in Eqs. (13)-(18) (Section II)

V_d Channel average electrode drop

v_1, v_2 Functions appeared in Eqs. (13)-(18) (Section II)

x, y, z Coordinates

α Hall angle

γ Specific heat ratio

Δ V_d/uBd = dimensionless electrode drop

θ Angle between the normal to the equipotential surface and the flow direction

ρ Density of the gas mixture

σ Scalar conductivity

τ Delay time

φ $E_y/E_x = \tan \theta$

Ω Hall parameter

2ρ Segmentation pitch

Subscripts x, y and z denote components in x, y and z directions, respectively. The bracket $\langle \rangle$ denotes average values.

I. INTRODUCTION

Since the time at which our first report AFAPL-TR-67-25 was issued describing the beginning of our work with diagonal conducting wall (DCW) generators, two-terminal operation has been investigated thoroughly. During this investigation two types of fuel were used; liquid combustion fuel and solid rocket propellant. The three DCW generators investigated were of identical geometrical configuration except for the side wall angles of 45°, 60° and 90°, respectively. The influence of side wall angle could thus be isolated from other effects and investigated over the same channel entrance conditions and magnetic field configuration for all generators. The comparative operation of these generators forms the basis for an extensive comparison of theory and experiment for DCW generators.

In addition to the over-all generator performance studies, efforts in the investigation of a variety of physical phenomena connected with generator operation were undertaken. For example, electrode phenomena were studied by means of high speed photography of the electrode surface leading to the discovery of arc-spots on the cathode. Two electrodes were segmented, one parallel and one transverse to the flow direction in order to measure current distributions on the electrodes. Great emphasis has been placed on the detection of instabilities in the generators. In this instability investigation current signals were recorded on high-speed tape simultaneously from different locations along the channel and their cross correlation investigated.

In addition to the experimental efforst outlined above, theoretical work was performed to include the effect of finite segmentation of the electrodes and to refine the model for the electrode drop. Future studies will include an investigation of the current flow to the side wall of the generator and its influence on generator performance, and also the boundary layer influence on current distribution.

II. GENERATORS USING LIQUID FUEL

II.1. INTRODUCTION

In this section we shall present experimental results
of two-terminal operation of a 60° diagonal conducting wall
(DCW) generator and a Hall generator under identical gasdynamic
channel entrance conditions and magnetic field configurations.
The overall performance of these generators from open-circuit
to short-circuit conditions is discussed.

A quasi-one-dimensional analysis is employed to treat
the average gasdynamic properties along the channel. The elec-
trical quantities are first treated by assuming infinitely
finely segmented electrodes; later, the correction due to the
finite size of the electrodes is incorporated.

It was found that the losses in the MHD channel could
be represented by a factor reducing the induced emf of the
generator. For the DCW generators which we have studied, tak-
ing the factor as a constant fraction of the induced emf, the
electrical properties can be predicted along the channel.
However, this simple representation of the generator losses is
not fully applicable over the whole range of external load con-
ditions from short to open circuit. A model for electrode
current dependent near-electrode sheath potential was then in-
troduced. It was found that such corrections enable us to
predict the whole operation range (from open to short circuit)
in the cases of the 45° and 60° generators, but that the agree-
ment is still not ideal for the Hall generator. The Hall
generator produces consistently less power than is predicted

II. GENERATORS USING LIQUID FUEL

by the theory, and the discrepancy increases as open circuit
is approached.

II.2. THEORETICAL STUDY OF TWO-TERMINAL CONNECTED GENERATORS

The DCW generators may be connected either by discrete
loads, as in the Faraday generator, or by two-terminal connec-
tion, as in the case of a Hall generator. Fig. II-1 illus-
trates the type of generator which is being investigated. The
series connection was first theoretically analyzed by de Montardy
(Ref. II-1) and its experimental performance first given in
Ref. II-2 and II-3. We now believe that DCW generators perform
in a different manner from the series connected generators
proposed by de Montardy. Evidence for this is contained in
the currents to the side walls described in Chapter IV. This
may mean that the DCW generators more closely conform to de
Montardy's assumptions than do the series connected generators
as currents to the side walls tend to maintain the diagonal
equipotentials in the channel. The various generator channels
are characterized by the angle θ. (Note here that the coordi-
nate system as shown in Figure II-1 is different from those in
Refs. II-4 and II-5). The Hall generator is then a special
case (corresponding to $\theta = 0$) of the family of DCW generators.

II.2.1. Theory for Infinitely Finely Segmented Electrodes

The electrical theory of infinitely finely segmented
electrodes with discrete loads was formulated in Ref. II-3.
Later, (Ref. II-4), it was found that the simple theory agrees
extremely well with the experiments provided an experimentally

determined electrode drop is included. The two-terminal load connection imposes the constant total current constraint,

$$I = \vec{j} \cdot \vec{A} = A(j_x + \varphi \, j_y) = \text{const.} \tag{1}$$

where A is the channel cross-sectional area and $\varphi = \tan \theta$, characterizing the type of channel as shown in Fig. II-1. With the aid of Eq. (1) we can find the corresponding resistivity r as

$$r = \frac{A}{I} uB(1 - \Delta)(\Omega + \varphi) - \frac{1}{\sigma} (1 + \Omega^2) \tag{2}$$

and the equivalent external load dR,

$$dR = \frac{r}{A(1 + \varphi^2)} \, dx \tag{3}$$

Summing over all the individual resistances we obtain the total load R_c as

$$R_c = \int dR = \int_{x_1}^{x_2} \left(\frac{dR}{dx} \right) dx \tag{4}$$

The other electrical quantities may be written in the following form for two-terminal connection

$$j_x = \frac{A\sigma uB(1 - \Delta)\varphi + (1 + \Omega\varphi)I}{A(1 + \varphi^2)} \tag{5}$$

$$j_y = \frac{A\sigma uB(1 - \Delta) - (\Omega - \varphi)I}{A(1 + \varphi^2)} \tag{6}$$

$$E_x = - \frac{A\sigma uB(1 - \Delta)(\Omega + \varphi) - (1 + \Omega^2)I}{\sigma A(1 + \varphi^2)} \tag{7}$$

$$E_y = \varphi \, E_x, \quad \text{where} \quad \varphi = \tan \theta \tag{8}$$

Here u is the flow velocity, B is the magnetic field strength, σ and Ω are the electrical conductivity and Hall parameter, respectively. All quantities are averaged values over the channel cross-sectional area, and hence, the only independent variable is in the flow direction x.

The average one-dimensional equations in a MHD generator channel may be written as follows:

$$\rho u A = \dot{m} \tag{9}$$

$$\rho u \frac{du}{dx} + \frac{dp}{dx} = -j_y B + dX \tag{10}$$

$$\rho u \frac{dH}{dx} = \vec{J} \cdot \vec{E} + dQ \tag{11}$$

$$p = \rho R T \tag{12}$$

and the electrical quantities are given by Eqs. (5)-(8). Here $\dot{m}$ is the mass flow rate and $H = h + \frac{1}{2} u^2$ is the stagnation enthalpy. The working fluid is a chemically reacting mixture, hence

$$R = \sum_i \frac{\rho_i}{\rho} R_i$$

$$h = \sum_i \frac{\rho_i}{\rho} R_i \quad \text{and} \quad h_i = \int_o^T C_{p_i}(T) dT + h_i^o$$

where subscript i denotes ith species, C_{p_i} is the specific heat a constant pressure, h_i^o is the beat of formation of ith species, and R_i is the gas constant. The species concentration ρ_i / ρ is determined by assuming chemical equilibrium. The electrical conductivity σ is computed using Frost's (Ref. II-6)

formulation. The frictional force dX and heat transfer dQ are not included in this study.

The one-dimensional equations in gasdynamics are extremely useful because of their simplicity. The theoretical validity of the one-dimensional formulation in the presence of the dimensional non-uniformities has been shown by Crocco (Ref. II-7).

The chemically reacting MHD one-dimensional equations can be integrated numerically with given entrance conditions and total current I provided the dimensionless electrode drop Δ is known. Fig. II-2 illustrates the method for determining Δ. A 45° channel was used with a total load of 15 ohms (loaded discretely), maximum magnetic field strength 1.9 Wb/m^2, mass flow rate .8 Kg/sec, entrance Mach number 1.5 and conductivity about 19 mhos/m The total power and voltage generated are 42 KW and 800 volts, respectively (test 23.4).

The one-dimensional equations along with the electrical relations are solved by using different values for Δ. The total power and voltage produced by this generator (operating at conditions where the experiments were performed) are plotted in Fig. II-2 for the 45° generator with discrete load as functions of Δ. It is obvious that the dimensionless electrode drop which best agrees with experiment is .56. It was shown (Ref. II-4) that this constant value indeed gave an excellent agreement between the theory and experiment (for discrete load) everywhere in the channel despite the fact that Δ was determined from the overall performance of the generator.

Consequently, the effective loss of uBd in the MHD channel seems to be everywhere proportional to the local induced emf. Due to the way in which Δ was determined, it is clear that it must represent all the losses existing in the channel. Although we are unable to separate exactly all the different loss mechanisms at present, it is important to find out what the fundamental influencing parameters are

Fig II-13 is a comparison of theoretical and experimental voltage distribution along a 60° DCW generator with two-terminal connection. The agreement is good. There is a slight difference in the load used in the experiment and the load used in computation. The center load was 9.8 ohms for the former and 9.5 ohms for the latter. This slight difference may be responsible for the lower predicted voltage output. The reason for the slight difference in loads is that in the calculation the total current is specified rather than the center load R_c.

The good agreement obtained by using the same value for Δ is shown in Fig. II-3, and this clearly indicates that the electrode drop in the 45° and 60° DCW generators, operating at similar load conditions, is the same. Furthermore, the type of loadings, whether two-terminal or discrete, does not affect the losses present in the generators.

Fig. II-4 shows the calculated voltage-current characteristic over the entire load spectrum for a Δ of .56. The experimental values are also shown for the purpose of comparison.

In the load range from 3 ohms to 10 ohms, the agreement between theory and experiment is good. However, at lower and higher loads deviations are shown. The value of $\Delta = .56$ was determined for a particular load, yet it does give a reasonable result for a range of loading conditions. Thus, one val'_ of Δ is unable to represent precisely the losses occurring in the generator from short to open circuits. This finding leads us to the investigation of the current dependent electrode drop which will be presented in the next section, and the influence of the finite segmentation which will also be examined.

II.2.2. Finite Segmentation of Electrodes and Influence of a Current Dependent Near-Electrode Sheath Potential

Homogeneity of the electrical properties over a cross-sectional surface of the generator is strongly dependent on the ratio of segmentation length 2ρ to the electrode distance d in y-direction. This ratio $2\rho/d$ varies in all of our three generators from 0.15 at the channel entrance to 0.1 at the exit of the generator.

Theories of Dzung (Ref. II-8), Witalis (Ref. II-9), and Schultz-Grunow and Denzel (Ref. II-10) show that, for parameters $2\rho/d$ ranging between 0.1 and 0.15 and Hall parameters Ω between 1 and 2, the influence of a discrete electrode and isolator on the performance of a cross-connected generator is also a strong function of the type of generator used. In Figs. II-5 to II-7, the influence of this geometrical effect on the normalized voltage-current characteristic is shown for each of

our three generator types. A comparison of these diagrams in-
dicates that the reduction of the generator voltage is the most
serious in the Hall generator.

In Chapter IV it will be seen that fair agreement is
obtained between the theory in Ref. II-9 for the current dis-
tribution over the electrodes in the Hall generator. In the
foregoing calculations of the voltage-current characteristic
for the different generators, the previously introduced factor
Δ was assumed to be independent of the electrode current I_e.
To include the physical phenomena at the electrode-plasma inter-
faces, the following model will be used: the near-electrode
layer is replaced by a potential discontinuity surface whose
potential difference is dependent on the electrode current.
The potential and current distributions within the channel
with the new boundary conditions at the electrodes have then
to be re-evaluated. In Fig. II-8 a part of the generator,
with cross-connected electrodes including the potential discon-
tinuity surfaces at anode and cathode, is shown.

With $V_d(I_e)$ as the sum of the potential discontinuities
at anode and cathode, the total generator current I and the
electrode current I_e then can be expressed by the relations

$$I = \sigma uBA \left(1 - \frac{V_d(I_e)}{uBd} \right) \tag{13}$$

$$\cdot \frac{(\frac{a}{d} - \frac{2\rho}{d} u_1) + (1 + \frac{2\rho}{d} v_1) \tan \epsilon}{(\frac{a}{d} + \frac{2\rho}{d} u)(\Omega - \tan \epsilon) + (1 + \Omega \tan \epsilon)(1 + \frac{2\rho}{d} v_2)}$$

and

$$l_e = \sigma uBA \, \frac{2\rho}{d} \left(1 - \frac{V_d(I_e)}{uBd} \right) \tag{14}$$

$$\cdot \; \frac{1}{(\frac{a}{d} + \frac{2\rho}{d} u_2)(\Omega - \tan \epsilon) + (1 + \Omega \tan \epsilon)(1 + \frac{2\rho}{d} v_2)}$$

where $\tan \theta = a/d$ represents the type of internal connection, and u_1, u_2, v_1, v_2 are dimensionless functions, given in Ref. II-8 or II-9, which depend on the electrode-isolator ratio and on the Hall parameter Ω.

In addition to these two equations we have the current dependence of the sum of the anode and cathode sheath potentials

$$V_d(I_e) = V_a(I_e) + V_c(I_e) = f(I_e)$$

Experimentally determined values representing this relation are known for different electrode temperatures (Ref. II-11), electrode materials (Ref. II-12), and magnetic fields up to 2.6 Wb/m^2 (Ref. II-13).

With these three relations, for each given generator current I, the generator operation parameter $\tan \epsilon$ and the electrode current I_e with the corresponding value for the sum of the sheath potentials V_c are determined. Using these values for $\tan \epsilon$ and V_d, we obtain for one segmentation length 2ρ of the generator:

Potential difference between two adjacent electrodes:

$$V_{2\rho} = 2\rho uB \left(1 - \frac{V_d(I_e)}{uBd} \right) \tag{15}$$

$$\cdot \; \frac{(\Omega - \tan \epsilon)}{(\frac{a}{d} + \frac{2\rho}{d} u_2)(\Omega - \tan \epsilon) + (1 + \Omega \tan \epsilon)(1 - \frac{2\rho}{d} v_2)}$$

Lorentz force:

$$(\vec{J} \times \vec{B})_x = -\sigma u B^2 \left(1 - \frac{V_d(I_e)}{uBd}\right)$$

$$(16)$$

$$\cdot \frac{1}{(\frac{a}{d} + \frac{2\rho}{d} u_2)(\Omega - \tan \epsilon) + (1 + \Omega \tan \epsilon)(1 + \frac{2\rho}{d} v_2)}$$

Gas power:

$$P_{in} = 2\rho A \sigma u^2 B^2 \left(1 - \frac{V_d(I_e)}{uBd}\right)$$

$$(17)$$

$$\cdot \frac{1}{(\frac{a}{d} + \frac{2\rho}{d} u_2)(\Omega - \tan \epsilon) + (1 + \Omega \tan \epsilon)(1 + \frac{2\rho}{d} v_2)}$$

Power output:

$$P_{out} = 2\rho A \sigma u^2 B^2 \left(1 - \frac{V_d}{uBd}\right)^2$$

$$(18)$$

$$\cdot \frac{\left[(\frac{a}{d} - \frac{2\rho}{d} u_1) + (1 + \frac{2\rho}{d} v_1) \tan \epsilon\right]\left[\Omega - \tan \epsilon\right]}{\left[(\frac{a}{d} + \frac{2\rho}{d} u_2)(\Omega - \tan \epsilon) + (1 + \Omega \tan \epsilon)(1 + \frac{2\rho}{d} v_2)\right]^2}$$

The dissipated power can be calculated as the difference between gas power P_{in} and power output P_{out}.

To demonstrate the additional influence of such an electrode current dependent sheath potential, the relation between V_d/uBd and I_e has been assumed to be linear in the range of electrode currents that correspond to the generator operation between open circuit and short circuit. As shown in Fig. II-9,

four different slopes (curve I to IV) for this dependence have been analyzed. In Fig. II-10 the effect of such a functional relation on the voltage-current characteristic of the 60° generator is presented. Because of the higher electrode currents at low loads in that type of generator, the voltage-current characteristic is dislocated to lower open circuit voltages. On the other hand, if the higher electrode currents occur at heavy load conditions of the generator, the voltage-current characteristic will be shifted to lower values of the short circuit current.

As indicated in Fig. II-10, the study of this effect leads to a better understanding of the experimental results of cross-connected generators. Since the change in electrode current is the most pronounced in the Hall generator, this special case of cross-connected generator suffers the most serious deviation from theory due to this effect.

II.3. OVERALL PERFORMANCE OF THE 60° DCW AND HALL GENERATORS

The propellants and aerodynamic conditions as well as the magnetic field configuration are kept the same for most of the experiments. The only variation is the external load conditions and the angles of the conducting side wall of the generators. Hence, it is possible to compare the various types of DCW generators over wide ranges of load conditions.

The main propellants used in the combustion chamber were RP1 and gaseous oxygen. The seed material was potassium. It was introduced in the form of potassium hydroxide (KOH) dissolved in ethyl alcohol (saturated at 56°F). The alcohol

concentration in the total fuel (alcohol is also being con-
sidered as part of the fuel) was 20% (by weight); this gave
the seed concentration about 1% (pure potassium). The com-
bustion chamber pressure was maintained at 46 psia which gave
a flow rate of about .8 Kg/sec. The generator entrance Mach
number was 1.5 and conductivity was 19 mhos/m. The average
test duration was about 8 seconds, with alcohol cut-off
occurring 2 seconds before engine shutdown. The magnet was
of conventional iron core construction, manufactured by Magnion,
which produced a maximum field strength of 1.9 Wb/m^2. The
length of the pole pieces was 36 inches. The uniformity of
the magnetic field over a channel cross-section was good.

Both the 60° DCW and the Hall channel have displayed
a remarkable endurance with little or no damage throughout
the experimental runs. The 60° wall channel operated for
nearly 1000 seconds during the 126 firings of one series while
the Hall channel operated for 600 seconds during 72 runs of a
single series (this inclueds runs with no seed and/or no mag-
netic field).

The channel construction is shown schematically in
Fig. II-1. There are 70 ammeters and 60 voltmeters which
provide instrumentation for monitoring wall currents, load
currents and load voltages as shown schematically in Fig. II-11.
A detailed description of the channel construction and instru-
mentation can be found in Ref. II-14.

The generator channels are of two-terminal connection
with a center load R_c. However, there are a few electrodes

in the entrance and exit regions of the channel connected by
discrete load in order to distribute the current load evenly
on the output electrodes as shown in Fig. II-11. The end
resistors are kept the same during most of the experiments
while the center load varies over a wide range. The influence
of the end resistor configurations has not been fully inves-
tigated yet. They contribute a small amount of voltage and
power output at the low center load operations, and at high
center loads this contribution is negligible.

The reproducibility of the time-averaged measurements
has been extremely good. Fig. II-12 shows the oscillograph
trace of the total voltage of the 60° DCW generator during
two tests under identical conditions. The Hall generator
exnibits a similar degree of reproducibility as recorded by
the low frequency (6 cycle) galvanometer. However, at higher
frequency (200 cycle), the above statement is no longer cor-
rect. The voltage trace for the galvanometer connected over
3/4 of the channel gives a ± 70 volts fluctuation (total
voltage output is about 600 volts) for the 60° DCW generator,
while for the Hall channel the fluctuation is ± 35 volts
over a total voltage output of 80 volts. This indicates that
a much higher percentage fluctuation exists in the Hall gener-
ator as compared to the DCW generators. The reasons for such
phenomena are not yet fully understood.

The overall performance of these two generators is
presented by the voltage-current characteristics as well as
the power output vs. center load plots. Fig. II-4 is the

voltage-current characteristic for the 60° DCW generator, while Fig. II-13 shows the power output vs. center load for both the 60° DCW and the Hall generators. It is clear from this figure that the 60° DCW generator produces three (3) times more power than the Hall generator at exactly the same gasdynamic entrance conditions and magnetic field strength. The voltage-current characteristics of the Hall generator are shown in Fig. II-14.

Figs. II-15 and II-16 show the voltage distribution along a 60° DCW generator when the center load is shorted and opened, respectively. The voltage distribution for the short circuit case exhibits an interesting S shape. (Note here the voltage output is not zero due to the end resistors.)

This interesting phenomenon indicates that part of the generator may operate as an energy sink (energy is being added to one part of the channel from other parts of the channel). This phenomenon occurs when the induced emf of the generator is less than the Hall voltage. Considering a Hall generator (only for its geometrical simplicity) $E_y = 0$ everywhere, and the Hall current is given by Ohm's law as follows:

$$j_x = \frac{\sigma}{1 + \Omega^2} \quad (E_x + \Omega u B)$$

In the case of two-terminal connection, we have the constant current constraint $I = \vec{A} \cdot \vec{J} = A j_x$ for the Hall generator. Then j_x is constant for a constant area channel; therefore, the voltage drop due to internal resistance remains the same. In normal operating conditions of a generator, the induced Hall emf ($\Omega u B$) is larger than the voltage drop due to internal

resistance; and, hence, the generator produces a positive vol-
tage gradient. However, if the induced Hall emf (ΩuB) is less
than the voltage drop due to internal resistance, the generator
will produce a negative voltage gradient and thus absorbs
energy. The following sketch demonstrates the two situations.

$$\Omega u B$$

$$E_x \qquad j_x \Big/ \dfrac{\sigma}{1 + \Omega^2}$$

Generator Mode

$$E_x \qquad \Omega u B$$

$$j_x \Big/ \dfrac{\sigma}{1 + \Omega^2}$$
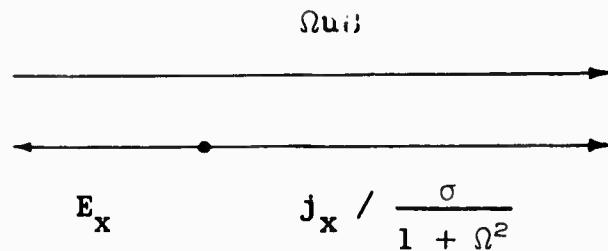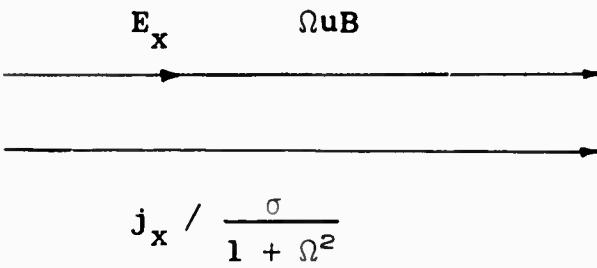
Energy Sink Mode

The negative Hall field condition occurs when ΩuB is
small. This corresponds to the two ends of a generator channel
where the magnetic field strength is decreasing. It is impor-
tant to note that the induced Hall emf decreased as B^2; there-
fore, the balance of the two voltages is very critical. For
a given generator channel and magnetic field configuration, the
energy sink mode more easily occurs at high current conditions
since the voltage drop due to internal resistance is large.

II.4. CONCLUSION

The governing equations for two-terminal connected generators were derived for both infinitely finely segmented electrodes and for those with finite segmentation. It was shown that the reduction of the generator voltage due to the finite size of the electrodes increases with increasing Hall parameter but decreases with increasing angle of the side wall. For the same Hall parameter, this influence is the most pronounced in the Hall generator.

Overall performance of 60° DCW and Hall generators in two-terminal operation was obtained over a wide range of load conditions. The experimental results show that the Hall generator produces much less (one-third) power than the 60° DCW generator under the same magnetic field configuration and channel entrance conditions. The reason for the poor performance of the Hall generator cannot be explained from the low value of the Hall parameter alone. Effort is now being taken toward the understanding of the Hall generator.

Calculations using a constant fraction of the induced voltage as an "electrode drop" have given a good representation of the electrical properties along the generators; however, the same constant factor gives precise agreement only for a restricted range of loads. The introduction of a current dependent sheath drop has demonstrated (Fig. II-11) that generator performance can be predicted over a wider range of external loads.

Finally we can conclude that the DCW generators are superior to the Hall generator in this range of operation.

The simple model employed here has shed sufficient light in
actual engineering design. However, future work must be con-
tinued to investigate the various physical phenomena that have
been omitted from the present theory.

REFERENCES

II-1. de Montardy, A., "MHD Generator with Series-Connected Electrodes," Proceedings of International Symposium on MHD Electrical Power Generation, Newcastle upon Tyne, 1962, Paper 19.

II-2. Dicks, J. B., "Design and Operation of Open Cycle Hall Current Neutralized MHD Accelerators and Generators with Diagonal Conducting Strip Walls," Proceedings of the Fifth Symposium on the Engineering Aspects of Magnetohydrodynamics, Massachusetts Institute of Technology, 1964.

II-3. Bugden, W. F. S., L. A. Green, J. Maycock, P. G. Meier, D. T. Swift-Hook and J. K. Wright, "Experimental Studies of the Performance of Long-Lived MHD Ducts," Proceedings of International Symposium on MHD Electrical Power Generation, Paris, 1964.

II-4. Dicks, J. B., Y. C. L. Wu, W. L. Powers, R. V. Shanklin, U. Zitzow, and R. E. Ziemer, " An Experimental and Theoretical Comparison of the Performance of Diagonal Wall Generators," Proceedings of International Symposium on MHD Electrical Power Generation, Salzburg, 1966, Paper SM-74/169.

II-5. Dicks, J. B., Y. C. L Wu, S. Witkowski, R. V. Shanklin, U. Zitzow, P. Chang, and R. E. Ziemer, "Characteristics of a Family of Diagonal Conducting Wall MHD Generators," Proceedings of Eighth Symposium on Engineering Aspects of MHD, Stanford University, 1967, p. 46.

II-6.   Frost, L. S., "Conductivity of Seeded Atmospheric Pressure Plasmas," Journal of Applied Physics, Vol. 32, 10, 2029, October, 1961.

II-7.   Crocco, L., "One-Dimensional Treatment of Steady Gas Dynamics" (ed, by H. W. Emmons), Princeton University Press, 1958.

II-8.   Dzung, L. S., "Gunstige Konfiguration der Segmentelektroden fur MHD-Generatoren," Brown Boveri Mitteilungen, 53 (1966), p. 238.

II-9.   Witalis, E. A., "Analysis of Linear MHD Power Generators," Journal of Nuclear Energy (Part C), 7 (1965), p. 455.

II-10. Schultz-Grunow, F., and Denzel, D. L., "The Electrical Characteristics of an MHD Generator Connected to an Arbitrary Load Resistance Network and the Experimental Determination of the Internal Conductance Matrix," Proceedings of International Symposium on MHD Electrical Power Generation, Salzburg, 1966, Paper SM-74/72.

II-11. Eustis, R. H., and R. Kessler, "Effects of Electrode and Boundary-Layer Temperatures on MHD Generator Performance," Ninth Symposium on Engineering Aspects of MHD, The University of Tennessee Space Institute, 1968.

II-12. Ogiwara, H., T. Tamaoki, and K. Mawatari, "An Experimental Study on Water-Cooled Metal Electrodes of MHD Generators," Ninth Symposium on Engineering Aspects of MHD, The University of Tennessee Space Institute, 1968.

II-13. Heurtin, J., and A. de Montardy, "Comportment d'Elec-
        trodes Metalliques dans une Tuyere MHD a Cycle Ouvert,"
        Proceedings of International Symposium on MHD Electri-
        cal Power Generation, Salzburg, 1966, Paper SM-74/79.

II-14. Dicks, J. B., Y. C. L. Wu, S. Witkowski, R. V. Shanklin,
        U. Zitzow, P. Chang, and R. E. Ziemer, "Diagonal Con-
        ducting Wall Generators," The University of Tennessee
        Space Institute, Technical Report AFAPL-TR-67-25.
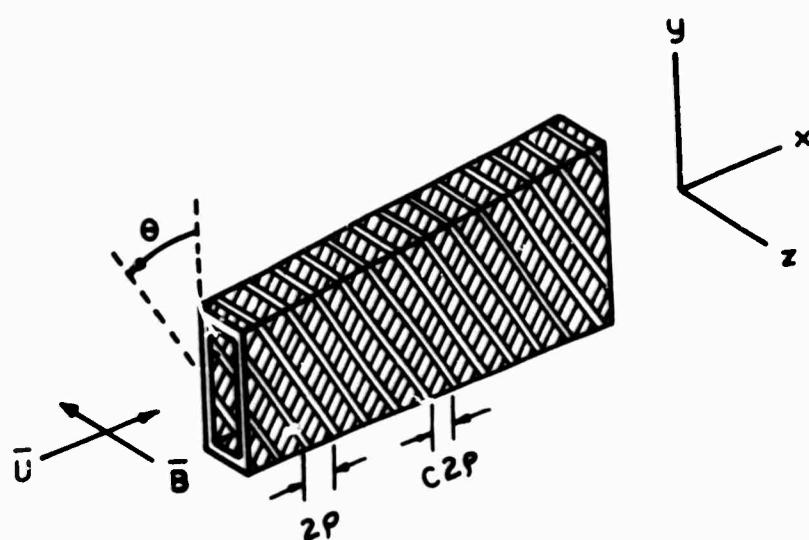
Fig. II-1 - Schematic Drawing of DCW Generator and Coordinate
System
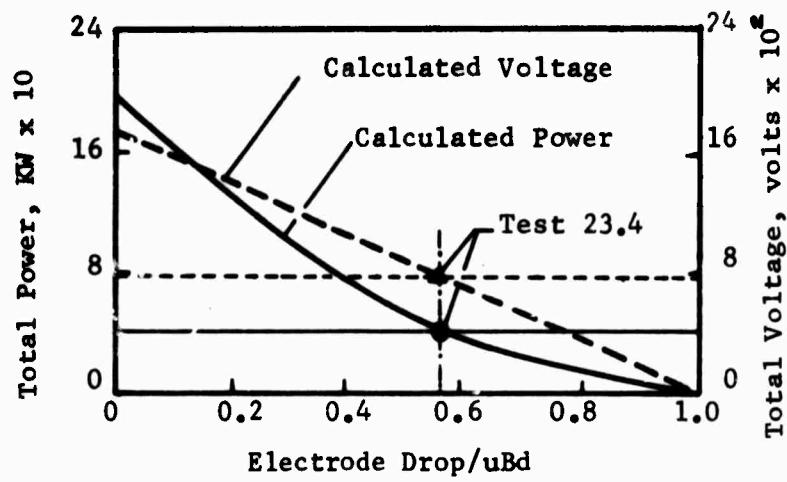
Fig. II-2 - Determination of Electrode Drop
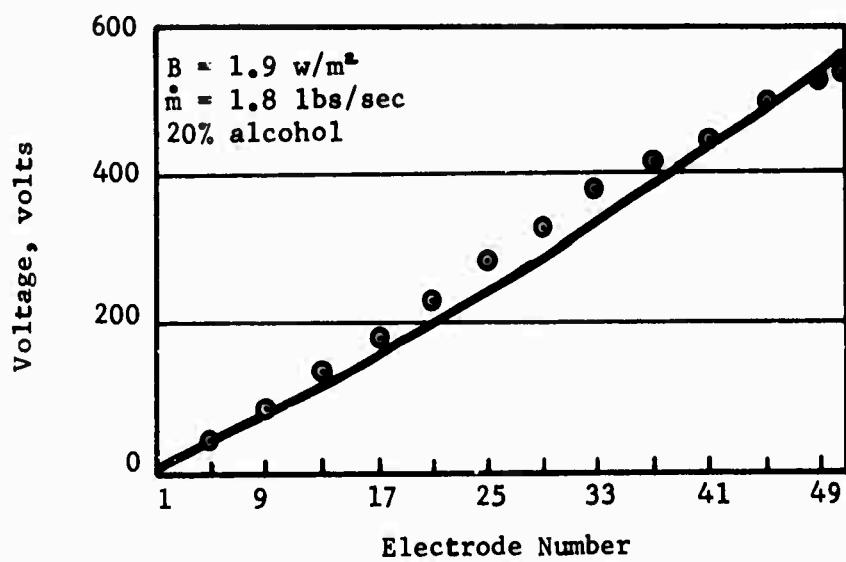
Fig. II-3 - Theoretical and Experimental Voltage Distribution along Channel
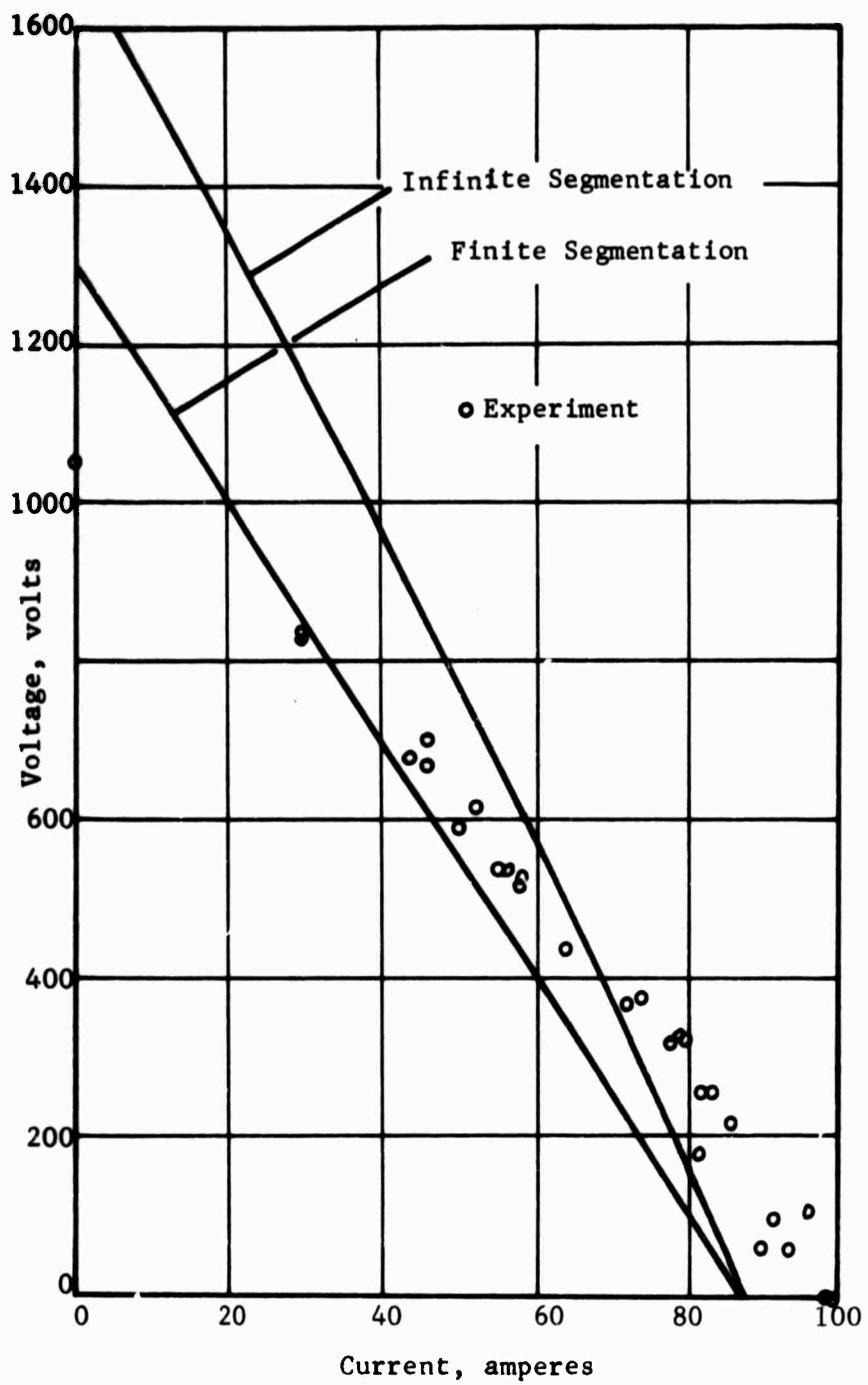
Fig. II-4 – Theoretical and Experimental Voltage-Current
Characteristics of 60° DCW Generator
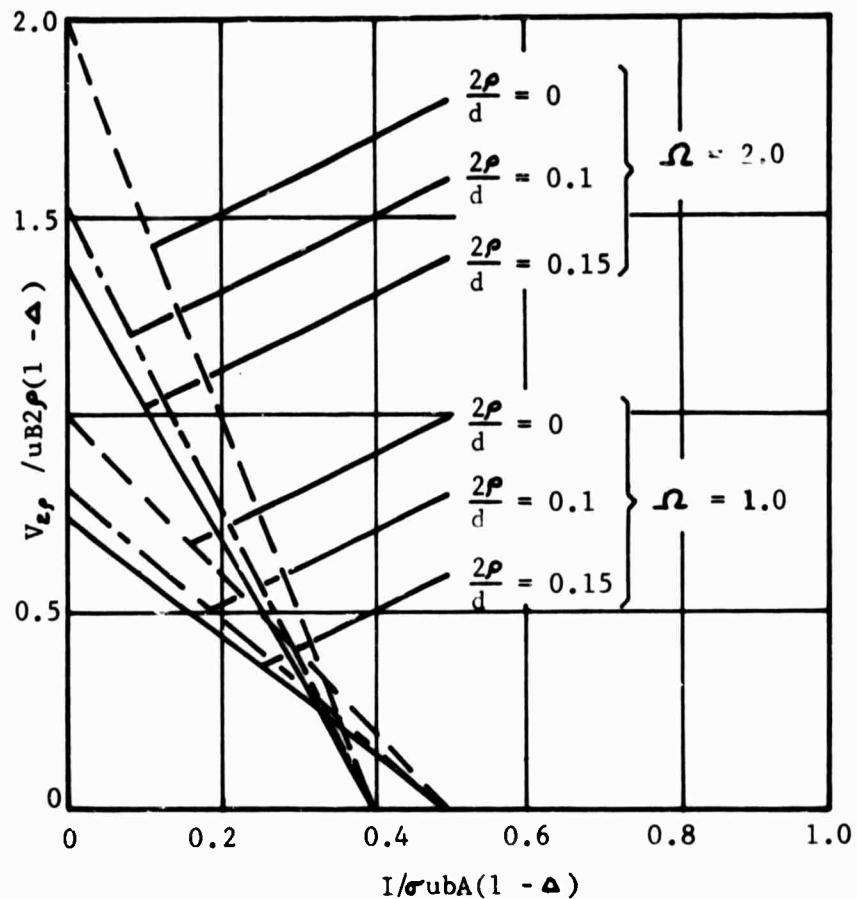
Fig. II-5 - Influence of Finite Segmentation on the Voltage-
Current Characteristic for Hall Generator
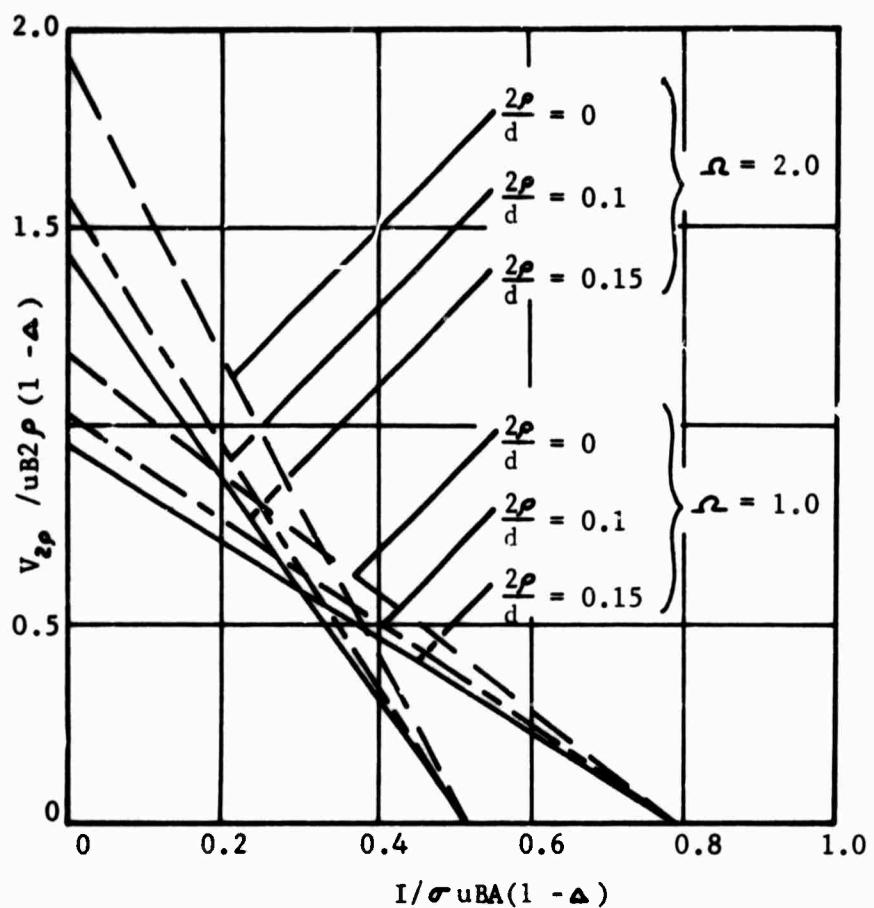
Fig. II-6 - Influence of Finite Segmentation on the Voltage-
Current Characteristic for 60° DCW Generator
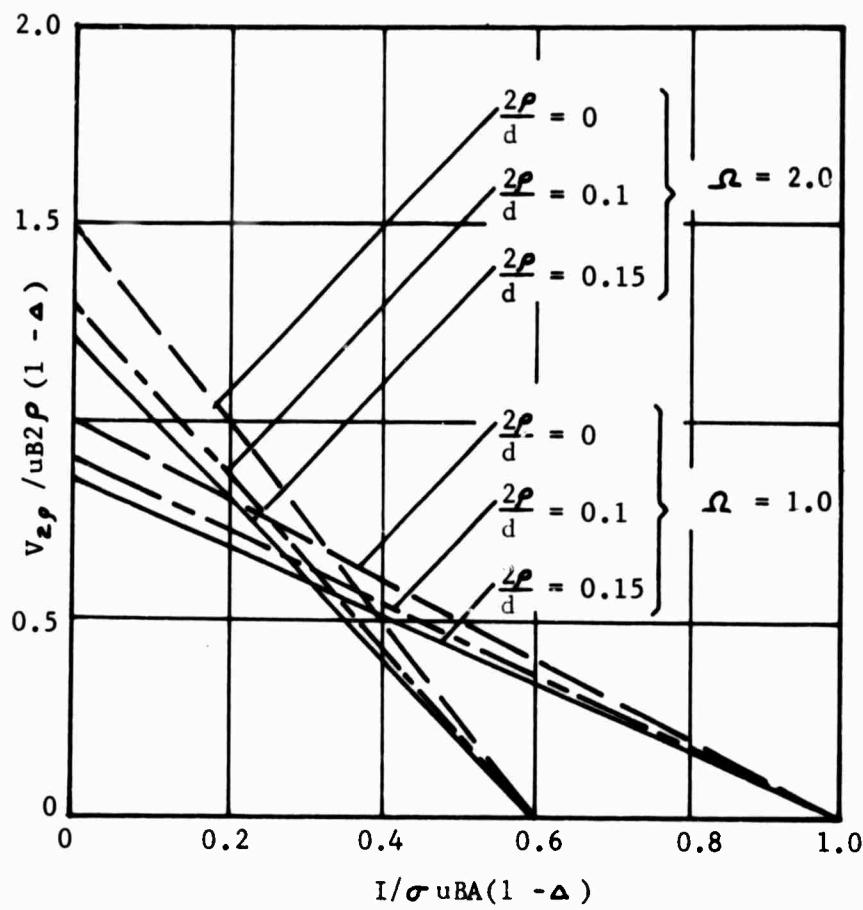
Fig. II-7 -- Influence of Finite Segmentation on the Voltage-
Current Characteristic for 45° DCW Generator
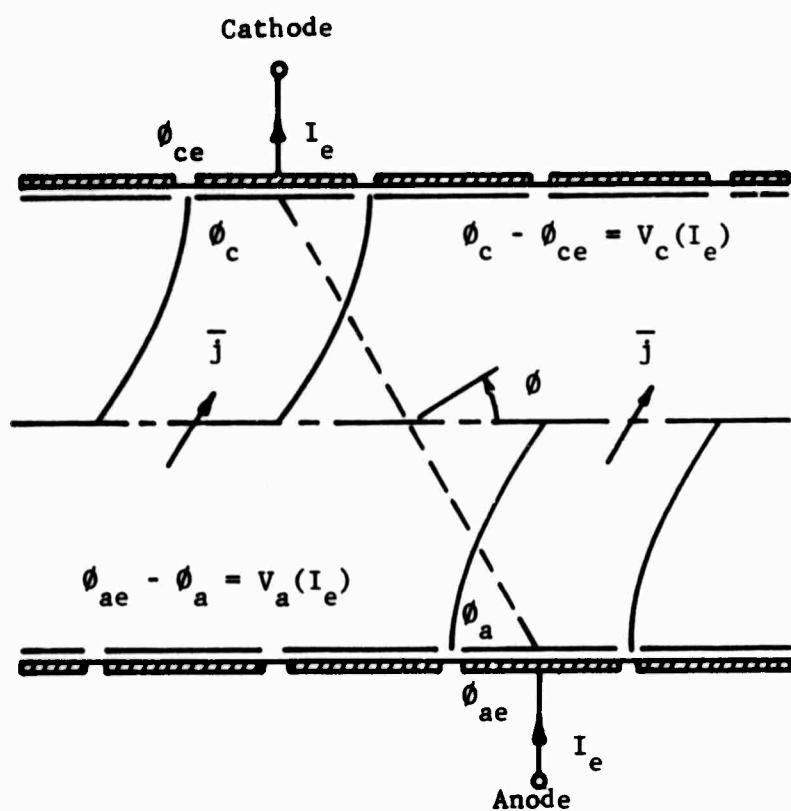
Fig. II-8 - Model for Current Dependent Sheath Potential
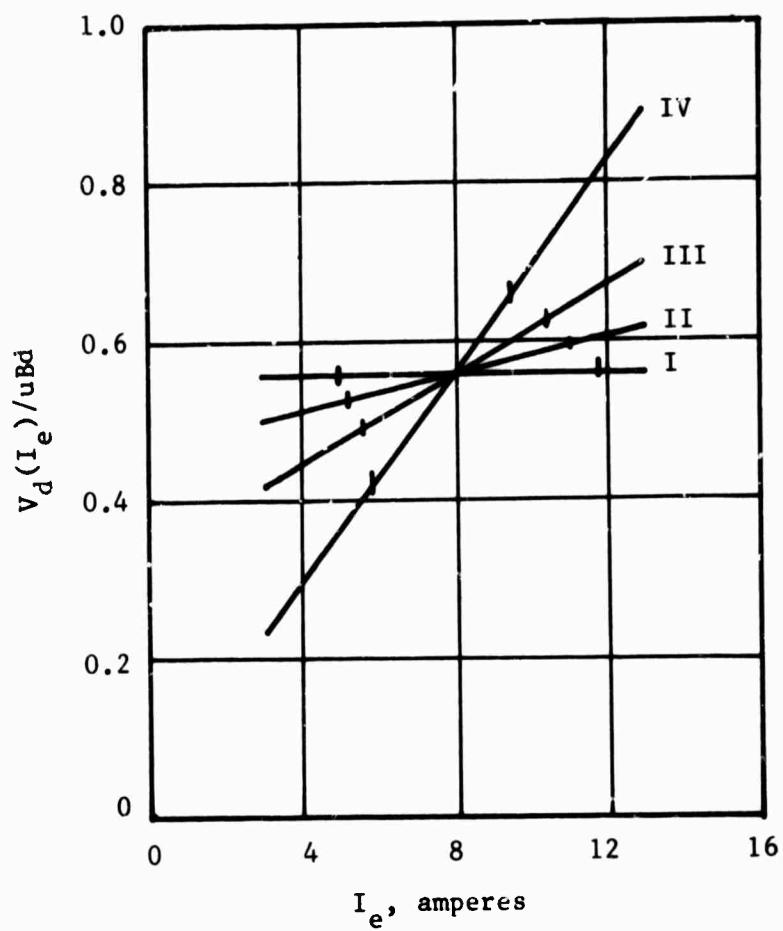
Fig. II-9 – Parametric Variation of Current Dependent Sheath
Potential
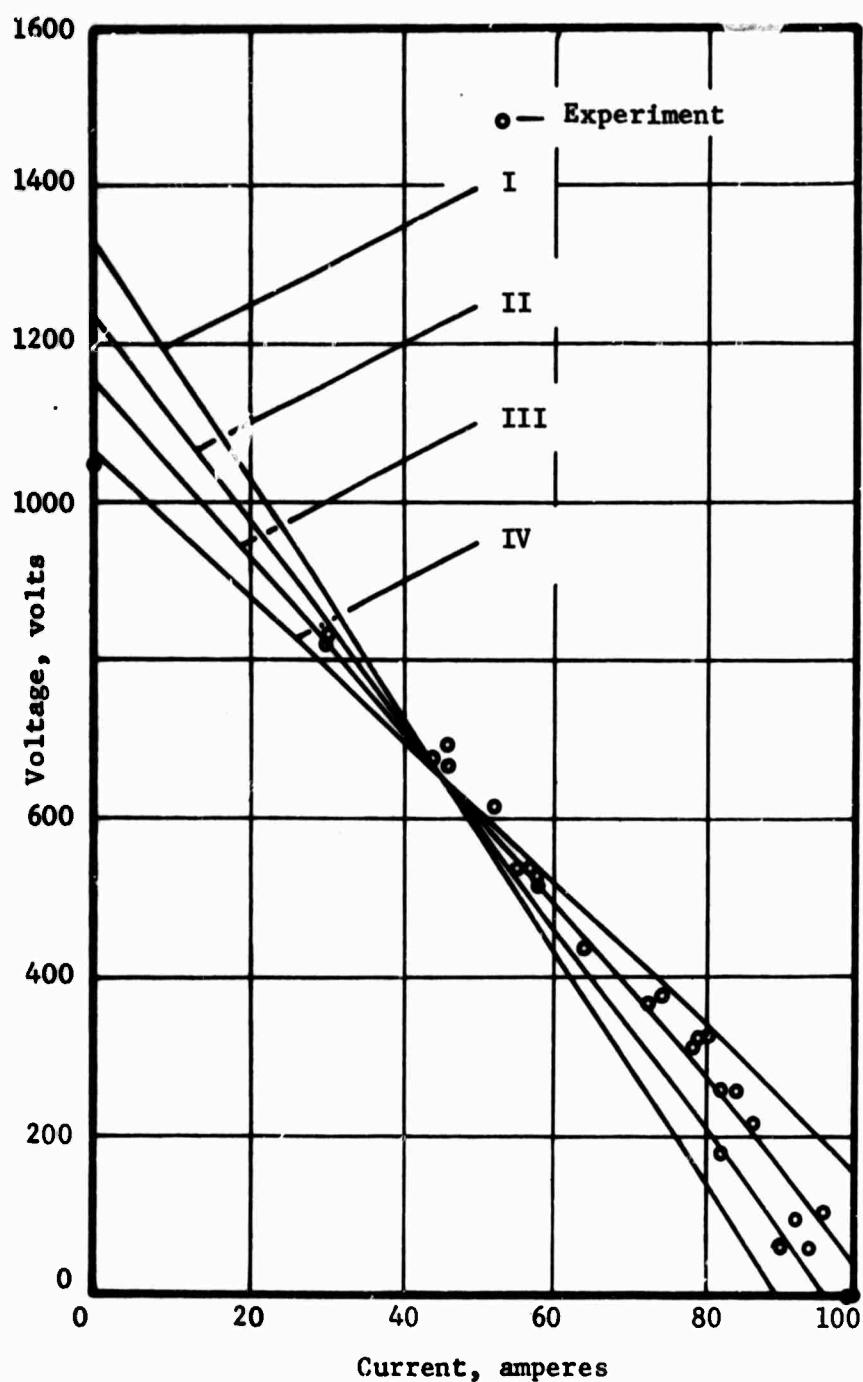
Fig. II-10 - Influence of Current Dependent Sheath Potentials on Voltage-Current Characteristic of 60° DCW Generator
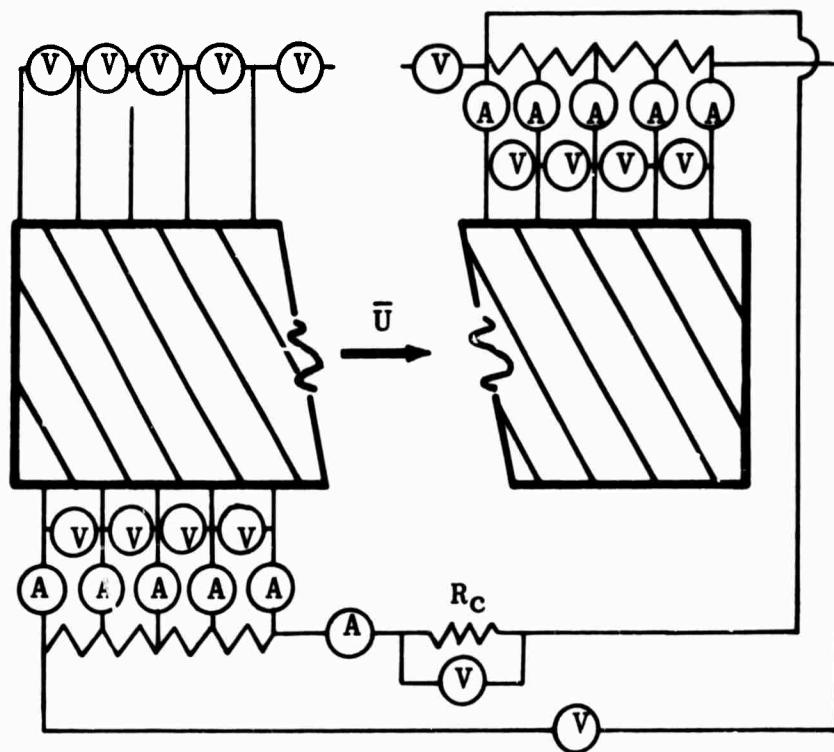
Fig. II-11 - Low Frequency Response Electrical Instrumentation
of 60° Channel
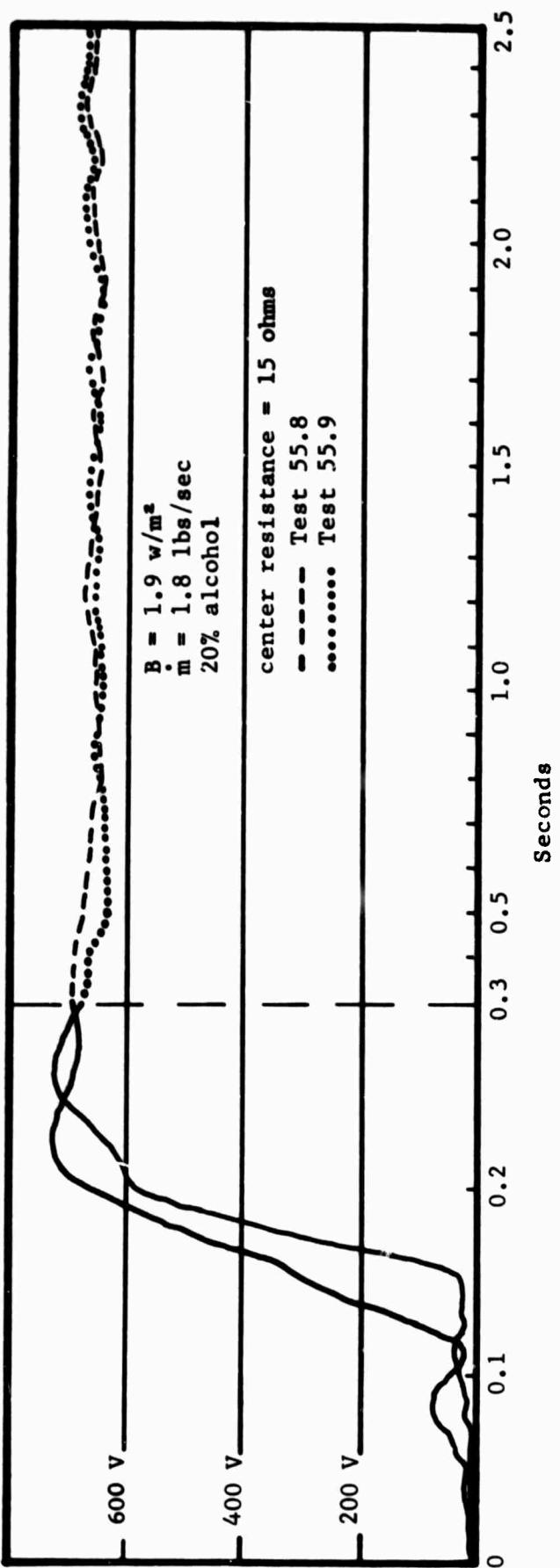
Fig. II-12 - Oscillograph Trace of 60° DCW Generator Voltage (6 Cycle Response)
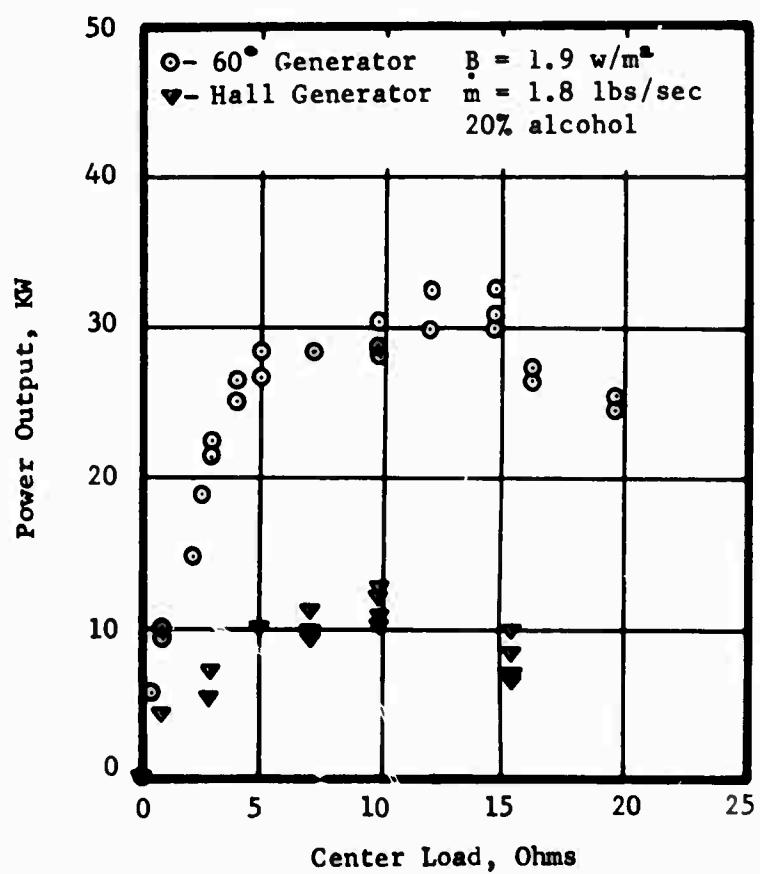
Fig. II-13 - Experimental Comparison of Power Output versus
Central Load of Hall and 60° DCW Generator
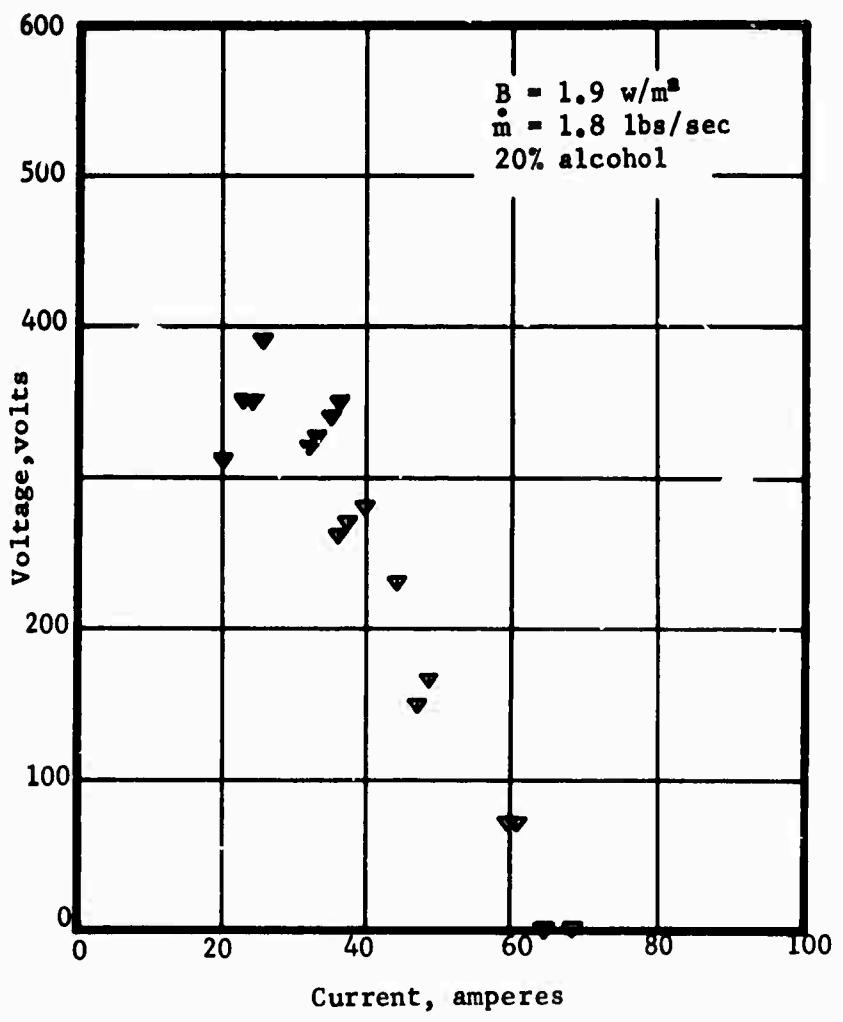
Fig. II-14 – Experimental Voltage-Current Characteristics of Hall Generator
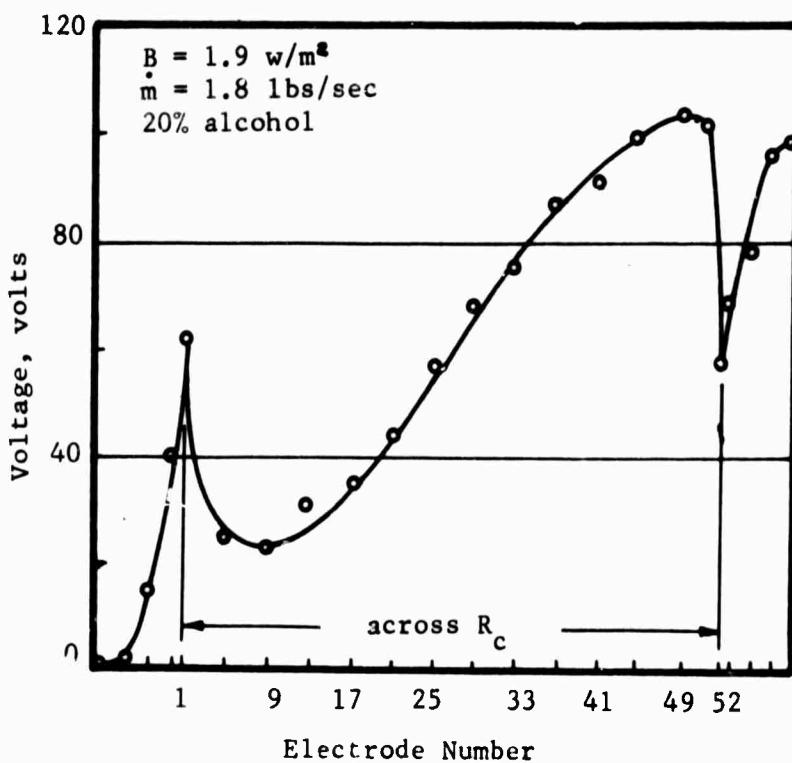
Fig. II-15 – Voltage Distribution along Channel at $R_c = 0$
(Short Circuit)
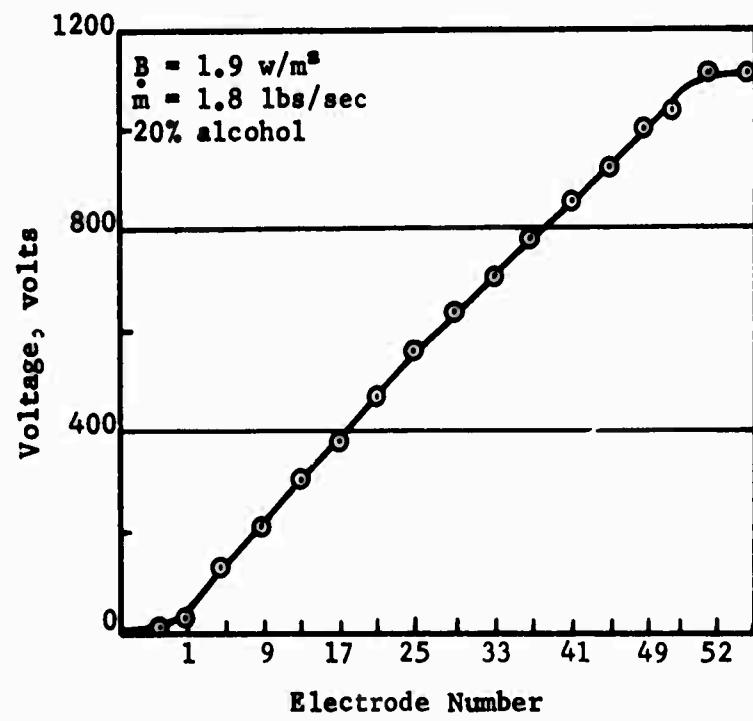
Fig. I.-16 - Voltage Distribution along Channel at $R_c = \infty$
(Open Circuit)

III. GENERATORS USING SOLID FUEL

III.1. INTRODUCTION

In this section we shall present the experimental results of a 45° diagonal conducting wall generator and a Hall generator using the combustion products of solid fuel as the working fluid. In addition, the Hall channel and the 45° channel have been used for an experimental determination of the conductivity and electron mobility of the working fluid.

The solid fuel was of a type similar to the double base metallized fuel used by Hercules, Inc., for other applications, except for the high potassium loading (5%). Operation of the same fuel under different combustion chamber and channel entrance conditions is discussed in Ref. III-1. The solid combustor utilized a cylindrical core solid rocket motor operating at 350 psia through a heat sink graphite nozzle and a transition section connected to the generator channel. The nozzle throat area was 3.2 sq. cms. with a channel inlet ratio of 16:1. The computations, performed by Hercules, Inc., indicated the following channel entrance conditions: mass flow rate, 0.68 kg/sec; pressure, 3 psia; gas temperature, 2000°K; Mach number 2.3; velocity, 2260 m/s; specific heat ratio, 1.33; electrical conductivity, 100 mhos/m; and an electron mobility of 1.1 m²/Vs.

III.2. CONDUCTIVITY MEASUREMENT

To measure the conductivity of the solid fuel plasma, a voltage of an external power supply was applied between

electrodes 3 and 7 and electrodes 54 and 58 of the Hall channel without magnetic field. The rest of the electrodes, isolated from each other, were connected to high impedance voltmeters as shown in Fig. III-1 and were used as floating potential probes. The electrodes which form the wall of the channel provided equipotential surfaces perpendicular to the plasma flow. The three voltages applied (200V, 340V and 440V) were chosen such that the resultant joule heating was small compared to the total heat energy released in the burning of the fuel. The voltages were still of sufficient magnitude to insure that the error reading of the individual potential differences was kept as small as possible.

Fig. III-2 illustrates a typical voltage distribution along the channel for an applied voltage of 340 volts. This potential distribution was observed to be nearly linear over the middle portion of the channel; however, the increase in electric field strength at each end of the linear portion of the magnitude observed cannot be attributed to the non-homogeneous current distribution near the feeding electrodes alone, but must also be connected with the physical phenomena at the cathode and anode.

Calculations of the conductivity were based on the differences in potential between adjacent electrodes where the regions of nonuniform current distributions have been excluded. With the potential readings along the channel and the measured total current I, the conductivity of the plasma was determined by Ohm's law,

$$\langle \sigma(x) \rangle = \frac{\langle j(x) \rangle}{\langle E(x) \rangle} = \frac{I \Delta x}{A(x) \Delta V(x)}$$

where $\Delta V(x)$ is the voltage difference between adjacent electrodes Δx apart, and $A(x)$ is the channel cross-sectional area at the position x along the channel axis.

Based on the above relation, the conductivity values have been determined for the three different applied voltages. The average values over the channel for the conductivity were observed to lie between 40 and 50 mhos/m.

The test results for all three applied voltages indicate the same tendency of a slightly increasing conductivity along the channel as it is shown in Fig. III-2. The increasing conductivity values may result from a slight increase in temperature along the channel duct. An increasing temperature of supersonic flow in a diverging duct can be explained only by heat addition to the flow resulting from exothermal chemical reactions in the duct. The occurrence of intense chemical reactions within the channel can also be supported by the physical condition of the channel after the conductivity tests. The chemical analysis of the deposits taken from the upstream part of the duct differs greatly in composition from those deposits taken from the downstream part of the channel.

III.3. GENERATOR EXPERIMENTS

III.3.1. Hall Channel

The Hall channel was installed for the solid fuel

tests with a two-terminal load connection and a central load resistance of 6 ohms. Due to observed channel conditioning effects (Ref. III-2) during previous liquid fuel experiments, it was deemed necessary to test first the Hall channel under the same load condition to determine if consistent results could be achieved for consecutive tests. In Fig. III-3 the overall performance for the first three power tests beginning with the clean, reinsulated channel is given. The results of tests 85.1 and 86.1 were considered to be close enough to conclude that repeatable results had been achieved after one test of the solid motors.

The data also indicates that the first test (84.1) produced more power than the subsequent power runs. This result was just the opposite of that observed during the previous liquid fuel tests where the first experiment of a series starting with the cleaned channel always produced lower power output than the later tests. In the liquid fuel case, this behavior in the difference of power output could be explained by a change of the electrode characteristic due to seed deposits on the electrode surfaces. The observed thickness of the deposit in the liquid fuel tests was not sufficient to allow local shorting between electrodes of the generator. After the first experiment with the solid fuel engine, the build-up of 2-3 mm thick layer of deposit covering the interior of the channel was observed. The thickness of this layer did not change significantly over a test period of more than ten experiments. It has been

observed that part of this deposit breaks away from the elec-
trode walls and part melts on the electrode wall and is re-
placed by a new layer of deposit during the same test. A
process of erosion and build-up has been confirmed by high-
speed photographs taken of the electrode surface during
experiments. Apparently the surface deposit of conductive
material built up during the first test reduced the performance
of the generator slightly for subsequent experiments, either
through leakage or through resistance offered to the electrode
current or both. This deposit stabilized completely after
the first run.

Fig. III-4 illustrates generator voltage, conductivity
and combustion chamber pressure traces recorded during tests
85.1 and 88.1. It was noted that in all tests the generator
voltage was nearly constant during the first 3 seconds of
the experiment while during the final 2-3 seconds the voltage
started to fluctuate. The mean value of the voltage taken
over this final period of the test time was always observed
to be higher than the voltage obtained from the constant
portion of the trace. Examination of the gasdynamic proper-
ties and conductivity during the test time revealed no
correlation with the voltage behavior. The only possible
explanations left were to assume that phenomena occurring
at the electrode surface were creating a reduction in the
sheath potential at the electrode-plasma interface, and
that the channel had suffered during the process of erosion
and build-up of the conducting deposit, which acts as an

additional time-dependent discrete loading, especially
observed in the final 2-3 seconds of each test.

Careful study of the high-speed movies was made.
There were, in general, more large pieces of solids presented
in the flow during the fluctuating period; however, these
correlations are only qualitative. No exact timing correla-
tions seem to exist between the oscillograph and the high-
speed movies.

The low power output of the Hall generator, using
solid fuel having conductivity values of 40-50 mhos/m, leads
us to expect a small value for the Hall parameter. Comparable
power output with the Hall channel was achieved during liquid
fuel tests under similar gasdynamic conditions where the
conductivity was less than 20 mhos/m, and the Hall parameter
at the same external magnetic field was close to 1.6.

III.3.2. 45° Diagonal Conducting Wall Generator

The initial three tests of the 45° channel were per-
formed with a two-terminal load of 7 ohms. Again the first
experiment with the clean and reinsulated channel produced
the highest power. The results of the two following tests
under the same load conditions demonstrated the repeatability
of the experiment. Subsequent tests of the generator were
conducted with loads varying from short circuit to open
circuit. In Fig. III-5 the experimental results for the
operation points of this generator during the initial steady
portion (0-3 sec.) of the test are indicated. In the same

figure the mean values for the voltage and current over the
final fluctuating portion of the generator operation are
also indicated. The time variation of the generated voltage
for these experiments was similar to that observed during the
Hall generator tests.

The power output of the 45° generator at a central
load resistance of 3 ohms was 110 KW during the first 3
seconds of the test and improved to a time-averaged value of
130 KW over the final time period of the experiment. The
average power produced during the first test run with this
channel was 162 KW at a load resistance of 7 ohms. The
maximum power produced was 208 KW during part of one test.
Comparing these results with the power output of the liquid
fuel tests, it was seen that the solid fuel produced 3 to 4
times as much electrical power with the same channel and
magnetic field configuration.

III.4. ANALYSIS BASED ON INFINITELY SEGMENTED ELECTRODES

III.4.1. Average Voltage-Current Characteristics

We can estimate the voltage-current characteristics
of our generators based on average values. This can be done
because of the relatively low magnetic field strength, and
hence the interaction of the MHD effects on gasdynamics is
very low. This results in slowly varying plasma properties
along the channel. The nearly straight line voltage-current
characteristic for both the liquid fuel and solid fuel tests

further justified the use of average values to estimate the generator behavior.

For infinitely segmented generators using two-terminal connection, the generated Hall field is (Ref. III-3):

$$E_x = - \frac{A\sigma(uB - V_d/d)(\Omega + \varphi) - (1 + \Omega^2)I}{A\sigma(1 + \varphi^2)} \tag{1}$$

where V_d represents the electrode drop which is a lump loss due to all effects in the generator, A is the channel cross-sectional area, u is the velocity, σ and Ω are electrical conductivity and Hall parameter, respectively, d is the distance between electrodes, B is the magnetic field, I is the total current, $\varphi = \tan \theta$ characterizes the type of channels and θ is the angle between the x-axis and the normal of the conducting side wall. In the previous liquid fuel tests, we found good agreement between theory and experiments if V_d is a constant fraction of the induced emf.

The average generated voltage $< V >$ is simply:

$$< V > = - < E_x > L$$

$$= \frac{L}{1 + \varphi^2} \left[(< u > < B > - < V_d >/< d >)(< \Omega > + \varphi) \right]$$

$$- \frac{L}{< A > (1 + \varphi^2)} \frac{1 + < \Omega >^2}{< \sigma >} < I > \tag{2}$$

where $< >$ denotes the values averaged over the channel length. The slope of the $< V > - < I >$ curve is:

$$\frac{d< V >}{d< I >} = - \frac{L}{< A >(1 + \varphi^2)} \frac{1 + < \Omega >^2}{< \sigma >} \tag{3}$$

provided $< V_d >$ is not a function of $< I >$.

A great deal can be learned from the above equation. For a given generator, L (active generator length), A and φ

are fixed values. The slope of the $\langle V \rangle - \langle I \rangle$ curve depends only on $\langle \Omega \rangle$ and $\langle \sigma \rangle$ provided the electrode drop does not depend on $\langle I \rangle$. A change of the induced emf or electrode drop contributes only to a "shift" of the voltage-current characteristic. However, for a change of $\langle \Omega \rangle$, both the slope and the open circuit voltage are influenced. On the other hand, for different types of generators φ would be different. For the Hall channel, $\varphi = 0$ while $\varphi = 1$ for the 45° side wall channel; thus the $\langle V \rangle - \langle I \rangle$ curve in the Hall channel is twice as steep as the 45° channel under the same plasma properties. Fig. III-6 shows the slope of the $\langle V \rangle - \langle I \rangle$ curve as a function of $\langle \sigma \rangle$ and $\langle \Omega \rangle$.

The open circuit voltage and short circuit current can be easily calculated as follows:

$$\langle V \rangle_o = \frac{L}{1 + \varphi^2} \left[(\langle u \rangle \times \langle B \rangle - \langle V_d \rangle / \langle d \rangle)(\langle \Omega \rangle + \varphi) \right]$$

(4)

$$\langle I \rangle_c = \frac{\langle A \rangle \times \langle \sigma \rangle [(\langle u \rangle \times \langle B \rangle - \langle V_d \rangle / \langle d \rangle)(\langle \Omega \rangle + \varphi)]}{1 + \langle \Omega \rangle^2}$$

(5)

III.4.2. Determination of Hall Parameter

In the solid fuel experiments, the 45° channel was tested over the whole resistance range, while the Hall channel was tested at only one resistance in order to determine the reproducibility of results. Three non-power runs were also performed in the Hall channel to measure the effective electrical conductivity along the channel. The average conductivity for the three runs was between 40 and

50 mhos/m. The average Hall parameter in the solid fuel tests based on these experimental data can be determined.

The open circuit voltage and closed circuit current in the 45° channel runs were 935 volts and 500 amperes, respectively. From Eqs. (4) and (5) we obtain:

$$\frac{<V>_o}{<I_c>} = \frac{L}{<A>(1+\varphi^2)} \frac{1+<\Omega>^2}{<\sigma>} = \frac{935}{500}$$

and $L = .792$ m, $<A> = 6.45 \times 10^{-3} m^2$, $\varphi = 1$. From the above relation we obtain:

$$<\Omega> = .47 \qquad \text{for} \qquad <\sigma> = 40 \text{ mhos/m}$$
$$.61 \qquad\qquad\qquad 45 \quad ''$$
$$.73 \qquad\qquad\qquad 50 \quad ''$$

The average value of the Hall parameter is below unity for all values of the conductivity. The low power output of the Hall generator compared with the power produced in the 45° generator can be explained partly by the small value of the Hall parameter Ω.

We can further determine the average dimensionless electrode drop in the channel after knowing $<\Omega>$. The average magnetic field strength is 1.74 w/m², and the average velocity was assumed to be 1850 m/sec. We obtain the values of

$$\frac{<V_d>}{<u><B><d>} = <\Delta>$$ as listed in the following table:

TABLE I - Hall Parameter and Electrode Drop

Average Conductivity mho/m	Average Hall Parameter $<\Omega>$	Average Electrode Drop $<\Delta>$
40	.47	.50
45	.61	.54
50	.73	.57

The values of Δ obtained here are in the same order of magnitude as in the liquid fuel case (Ref. III-4) where $\Delta = .56$.

III.4.3. Computing the Voltage-Current Characteristic for the Hall Generator

The average voltage-current curve (straight line) is obtained by connecting the points of open-circuit voltage and closed-circuit current. Based on the values calculated in the above section, we find:

TABLE II - Hall Generator Performance Characteristics

Average Plasma Conductivity	Open Circuit Voltage (Volts)	Short Circuit Current (Amperes)
40	598	160
45	714	192
50	798	213

Fig. III-3 also shows the average voltage-current characteristics for the Hall generator. The calculated power output is slightly higher than the experimental values.

III.5. CONCLUSIONS

Two results of significance were obtained in these experiments. First, as shown in Fig. III-7, the generator power output was 3 to 4 times higher (despite possible incomplete combustion) than that achieved by a 20% higher flow rate using conventional RP1 and gaseous oxygen for the same generator channel. Second, the generators operated with relatively little effect observed w.en layers of

aluminum oxide and other chemicals from the fuel coated the wall as thick as 3 mm.

The experimental results showing that generators can run with aluminum oxide and potassium coating without large degradation in power is of great significance in the field of coal-burning MHD as well as solid fuel MHD. Coal or ash products, mostly aluminum oxide, coat the electrodes; and it was previously believed that this had a highly detrimental effect on power production. The experiments here indicate that this is not the case, with a relatively small increase in electrode drop observed and no indication of shorting or leakage currents between the electrodes noted. From high-speed motion pictures taken of this coating process, the above results were noted even in the presence of melted material covering the walls.

It is possible to speculate that not only does the coating fail to destroy generator performance, but it also may even increase generator lifetime by preventing electrode deterioration.

REFERENCES

III-1. Bangerter, C. D., A. H. Peterson, and E. D. Couvert, "Operation of Solid Fuel MHD Generators," Proceedings of the Eighth Symposium on Engineering Aspects of MHD, Stanford University, 1967.

III-2. Dicks, J. B., Y. C. L. Wu, S. Witkowski, R. V. Shanklin, U. Zitzow, P. Chang, and R. E. Ziemer, "Diagonal Conducting Wall Generators," Technical Report AFAPL-TR-67-25, The University of Tennessee Space Institute.

III-3. Wu, Y. C. L., D. L. Denzel, S. Witkowski, R. V. Shanklin, U. Zitzow, J. W. Muehlhauser, P. Chang, E. S. Jett, and J. B. Dicks, "Two-Terminal Connected Open Cycle MHD Generators," Ninth Symposium on Engineering Aspects of MHD, 1968.

III-4. Dicks, J. B., Y. C. L. Wu, S. Witkowski, R. V. Shanklin, U. Zitzow, P. Chang, and R. E. Ziemer, "Characteristics of a Family of Diagonal Conducting Wall MHD Generators," Proceedings of the Eighth Symposium on Engineering Aspects of MHD, Stanford University, 1967.
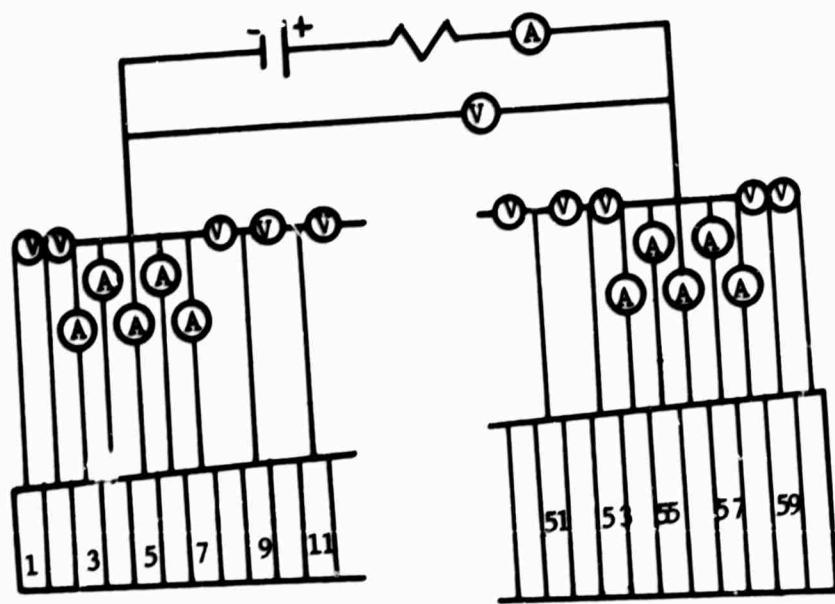
Fig. III-1 - Low Frequency Electrical Instrumentation for
Conductivity Experiment
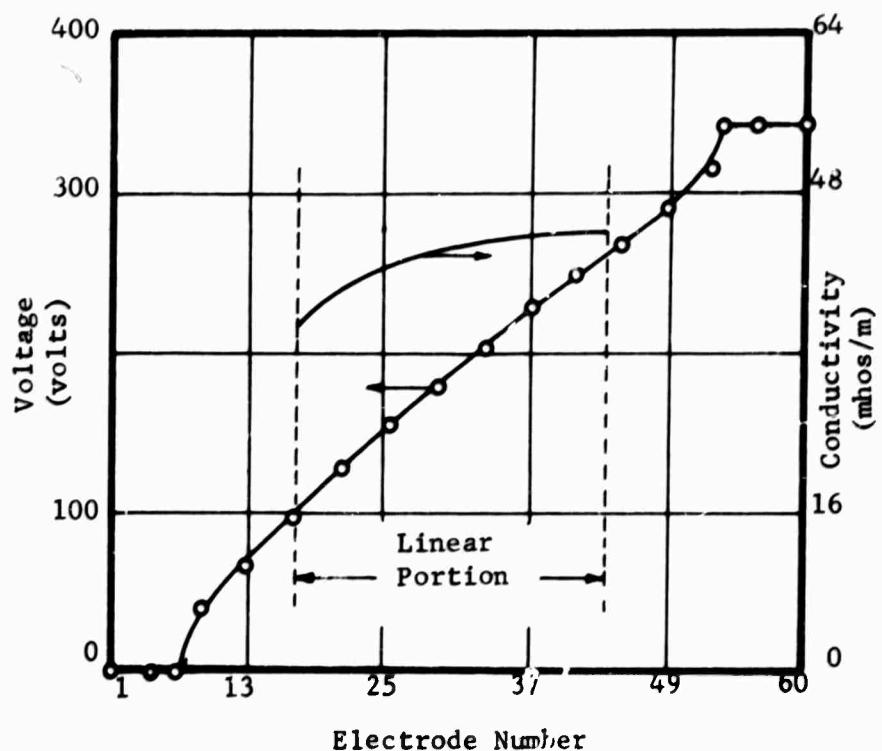
Fig. III-2 - Potential Distribution and Conductivity Measured
along Hall Channel at an Applied Voltage of 340V
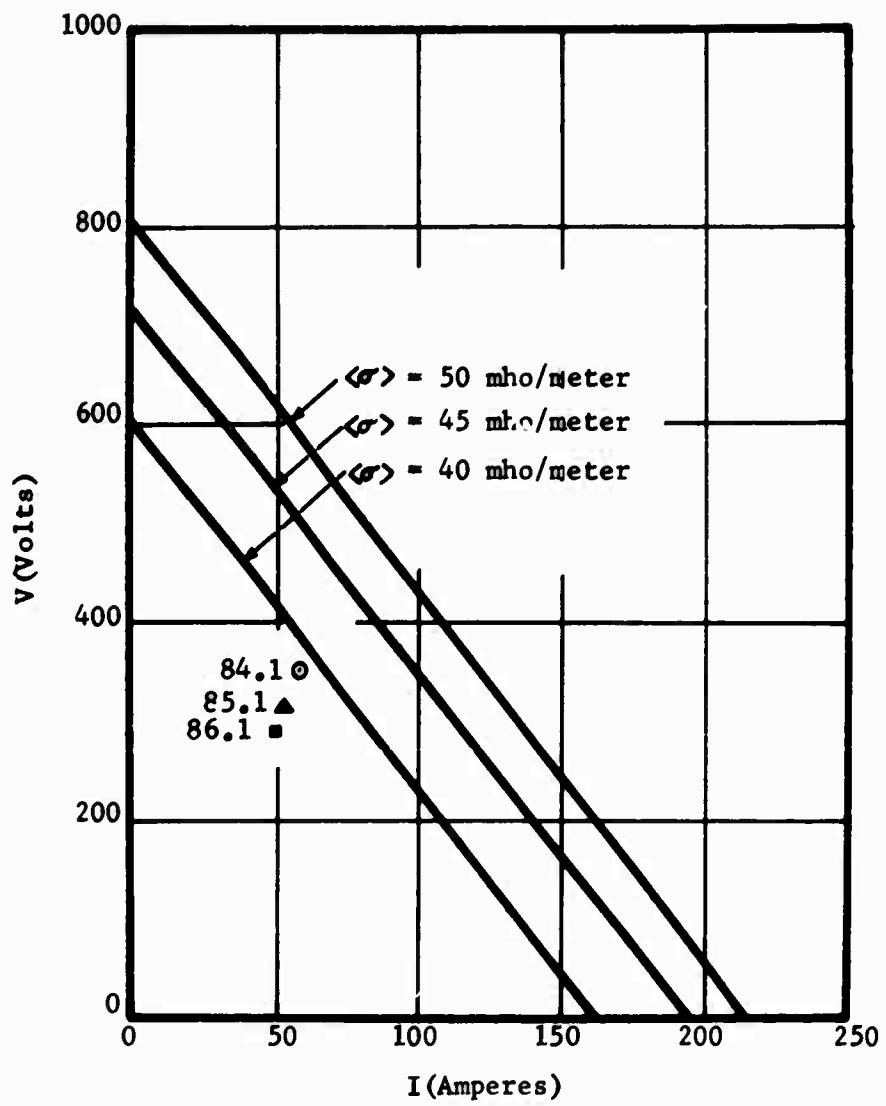
Fig. III-3 - Theoretical and Experimental Hall Channel
Performance
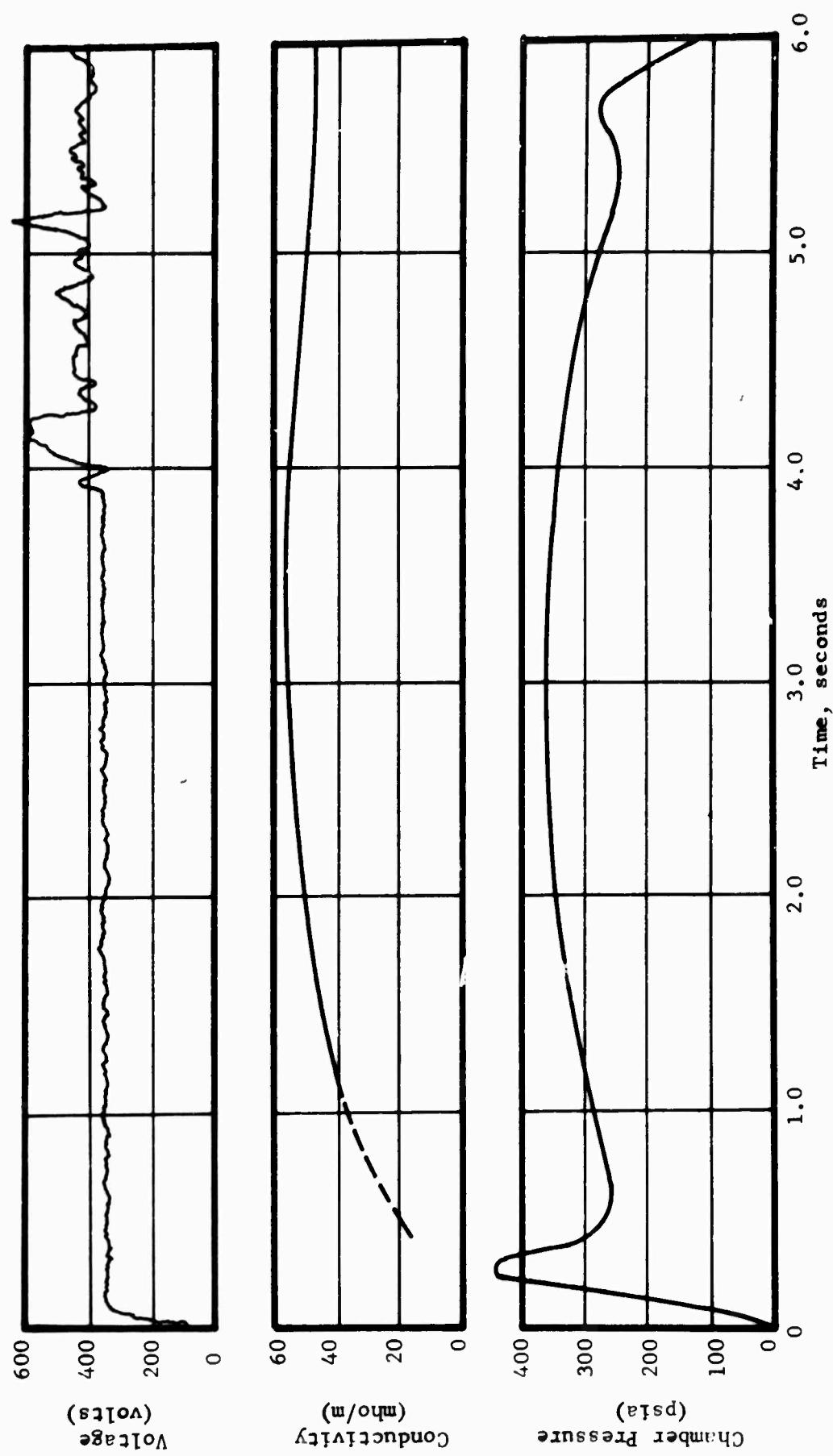
Fig. III-4 -- Comparison of Variation of Chamber Pressure, and Voltage Plotted over the Time of Test 85.1 with Conductivity of Test 88.1.

55
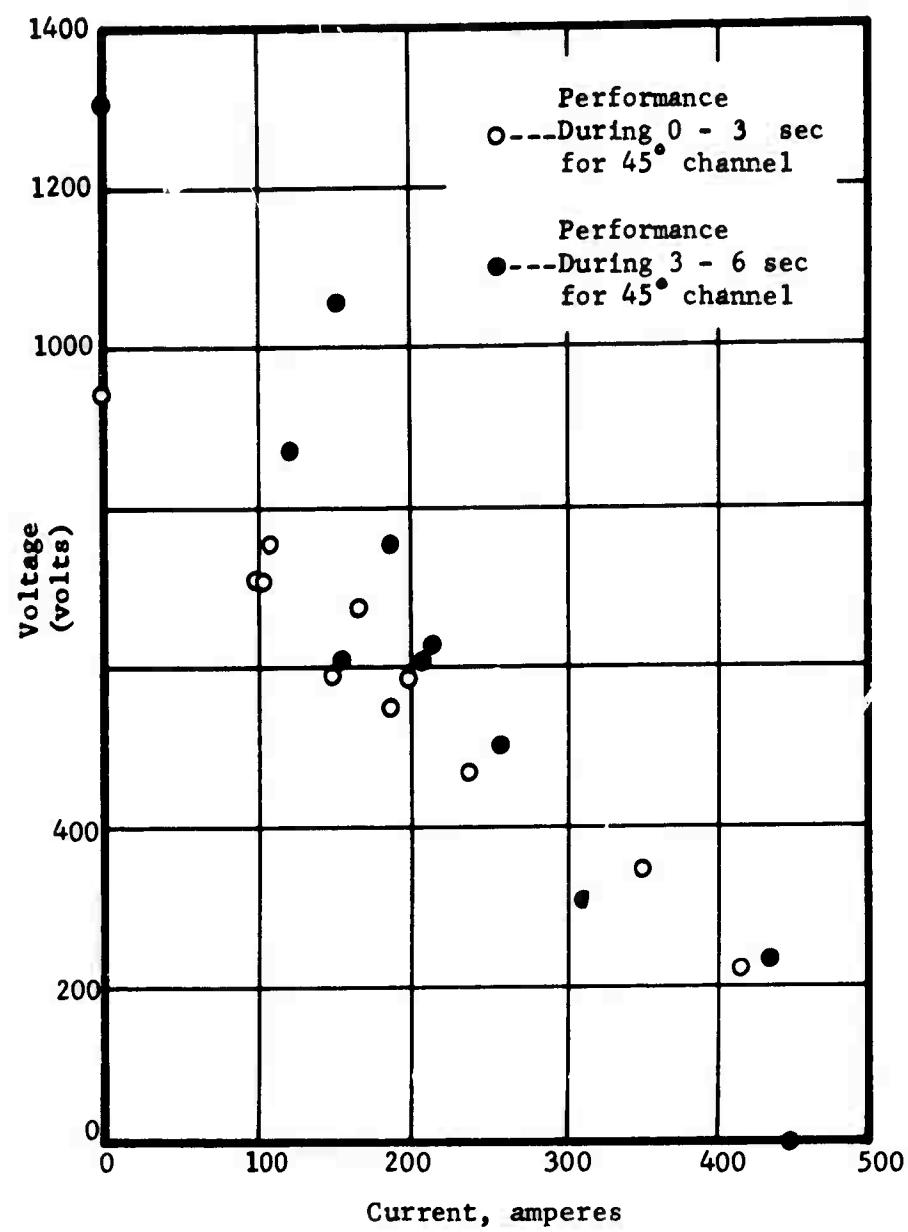
Fig. III-5 - Voltage-Current Characteristics for the 45°
            Channel Performance
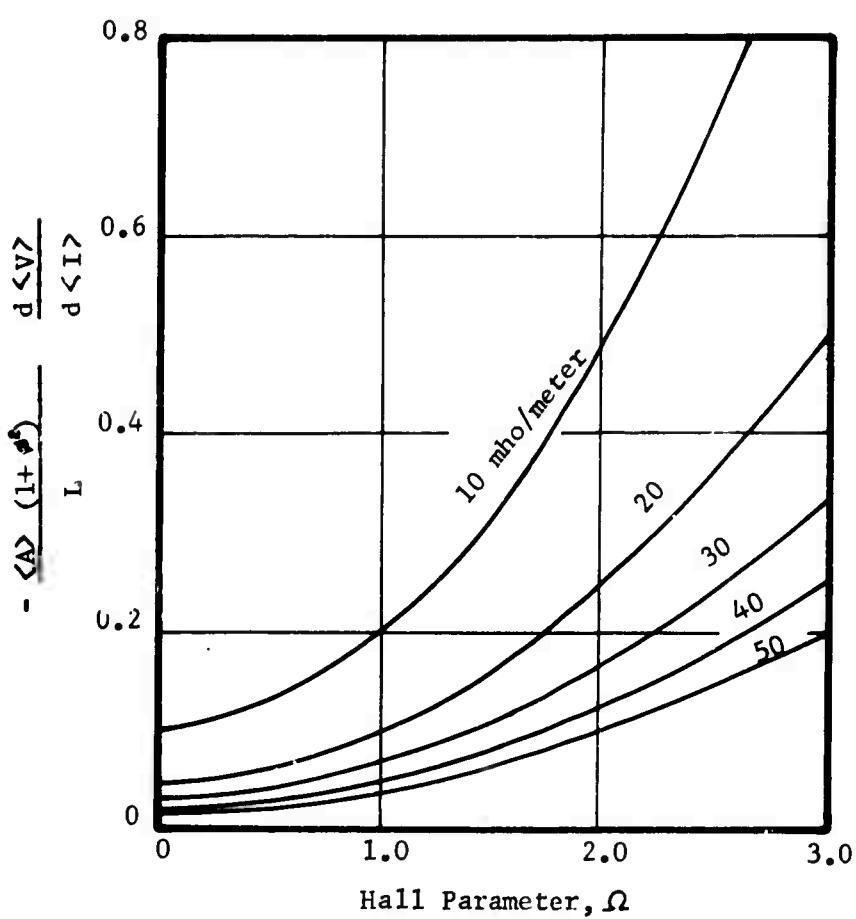
Fig. III-6 – Slope of the Average Voltage-Current Characteristic as a Function of Ω with the Conductivity as Parameter
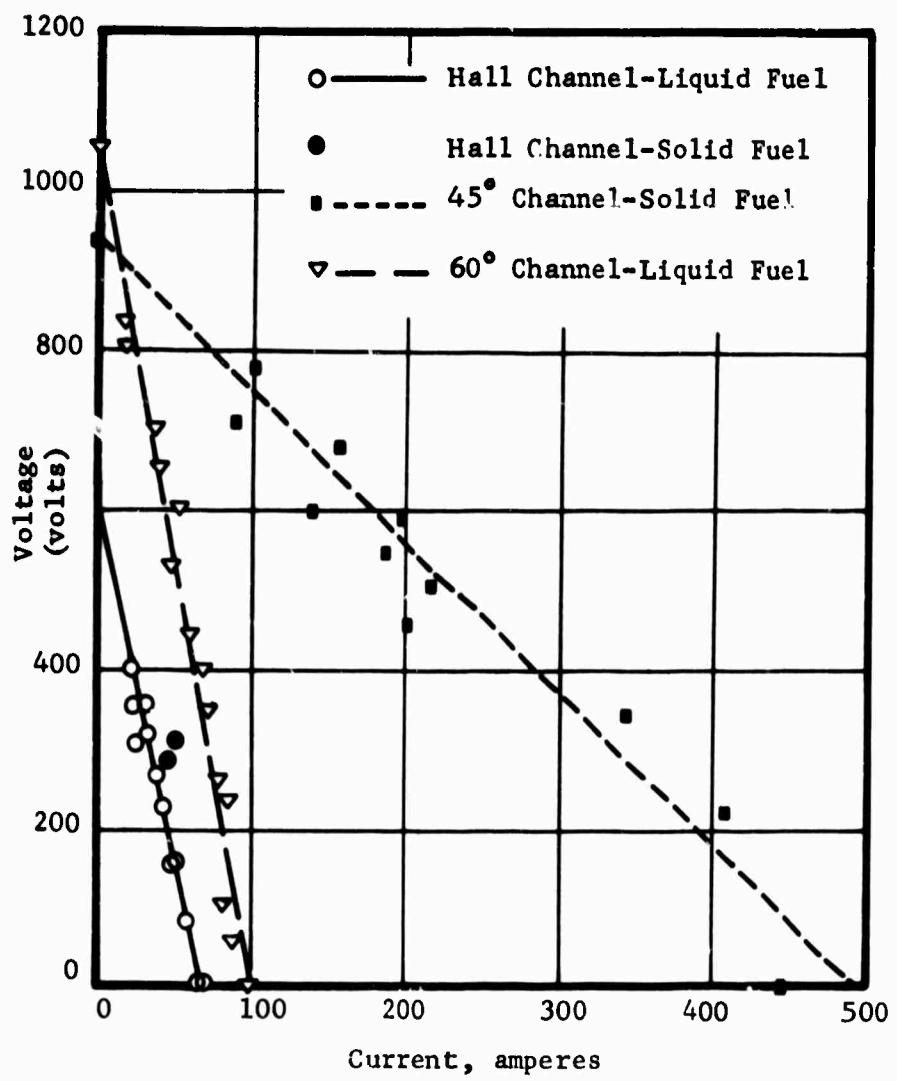
Fig. III-7 - Comparison of Diagonal Conducting Wall and Hall
Channels at Two-Terminal Load Conditions Using
Liquid and Solid Fuels

IV. ELECTRODE PHENOMENA

IV.1. INTRODUCTION

The experimental investigations in this section are concerned with the observation of electrode surface phenomena and measurements of the current distribution over the generator electrodes.

Besides the standard type of instrumentation as used in earlier experiments, in this series of tests new instrumentation and measuring techniques were applied:

1. A high-speed motion picture camera was directed on a tube connected with the top part of an electrode and focused on the internal surface of the bottom part of that electrode. By reversing the magnetic field direction, the observed electrode part could be operated as cathode or anode under the same gasdynamic and load conditions (Fig. IV-1).

2. Two of the 60 electrodes were divided in small segments in order to get more information on the current distribution of each of the individual electrodes. This subdividing of the electrodes was carried out in two different directions; one electrode with segmentation in the flow direction and the other electrode with segmentation in the magnetic field direction.

i .2. EXPERIMENTAL STUDY

In Fig. IV-1 the locations along the Hall channel of the two segmented electrodes and of the specially designed electrode with the observation window for the high speed camera are indicated.

Since all electrodes with this instrumentation were
in the homogeneous region of the external magnetic field, and
gasdynamic parameters do not vary greatly along the channel,
the obtained results should be representative for all the elec-
trodes except those few located in the entrance and exit regions
of the generator.

IV.2.1. High Speed Photographs of Cathode and Anode Surfaces During Generator Operations

A. Description of Instrumentation

Electrode No. 51 of the Hall channel has been especially
designed as illustrated in Fig. IV-2. This electrode was con-
structed in such a manner as to allow viewing of the interior
bottom surface through a 3/8 x 1-1/2 inch opening in the top
part. Cooling water (not illustrated in the schematic Fig.
IV-2) was provided around the opening in the top part to pre-
vent local overheating at the sharp edges exposed to the gas
flow.

A copper tube, sufficiently long to assure the correct
distance between the objective lens of the camera and the bottom
surface of the electrode, was attached to the opening in the
electrode. The top of this tube was sealed with a shatterproof
glass observation window. The high speed camera was mounted
directly over this window. The camera mounting was secured to
a laboratory frame which was independent of the channel and its
associated mountings to prevent channel vibrations from inter-
fering with camera stability.

Three No. 57 Wratten filters were used in the camera
to reduce the intensity of the spectral emission from the

potassium atoms. An additional neutral density filter was included to achieve a larger lens opening and hence to reduce the field of focus to the immediate region of the electrode surface. The camera was loaded with 400 feet of 16 mm black and white (Eastman RP Type 7229) or color film (Type 7258). Three seconds after ignition of the combustion chamber, the camera was set to run at 5000 frames per second. The total length of time of channel operation filmed under these conditions was approximately three seconds.

The electrical instrumentation for this electrode was identical to the other electrodes in the Hall configuration. The top to bottom electrode current was varied from 10 to 15 amperes at different runs by changing the load conditions of the Hall generator. By reversing the direction of the applied magnetic field, both the cathode and anode surfaces could be inspected.

B. Experimental Results

During the initial portion of the filmed results, before the film speed achieved its maximum rate, the cathode surface was observed to have spots of high luminosity along the upstream and downstream edges. These spots remained in the same position along the edges for relatively long time periods (100 milliseconds). No preference for distinct location along the edge was observed for these spots. However, when there was a spot visible on the downstream edge of the next upstream electrode, the same spot pattern usually occurred on the edge of the next downstream electrode.

When the camera came up to the desired speed of 5000 frames per second, moving spots over the cathode surface could be detected. The series of pictures illustrated in Figs. IV-3 and IV-4 show, as an example, such a cathode spot moving from the upstream edge to the downstream edge of the photographed electrode. With the time scale indicated beside each of the presented pictures, the velocity of this spot could be determined as $v_s \approx 1.0$ m/s. All observed cathode spots were moving in the flow direction with velocities of the same order of magnitude; their paths of motion were always found to be parallel to the gas flow.

The spots moving across the electrode started at a position where a stationary spot at the downstream electrode edge of the adjacent upstream electrode was already formed. Usually at the same time, three or four moving spots following each other with nearly equal spacing were observed on their paths across the cathode surface.

As a result of this observation most of the cathode current is thought to be carried through these spots. The observed direction of motion of the spots is in the flow direction and not in the $\vec{J} \times \vec{B}$ direction. When the magnetic field was reversed and the observed electrode served as anode, no spots were observed.

IV.2.2. Segmented Electrodes

A. Description of Instrumentation

To receive information about the current distribution over the electrodes of the Hall channel, the top parts of two

electrodes were divided into a number of identical pieces isolated from each other.

Electrode No. 22 (Segmented Electrode I) was subdivided parallel to the axial channel direction and consists of seven individual elements (Fig. IV-4). The top part of electrode No. 34 (Segmented Electrode II), divided transversely to the channel axis, was built of 10 elements (Fig. IV-5). The electrical isolation from adjacent pieces was achieved by means of 0.010" thick mica paper.

The electrical circuit arrangements of the two segmented electrodes are also indicated in Figs. IV-4 and IV-5. The electrical instrumentation shown consisted of 0.2 ohm shunt resistors and 1 mA/cm sensitivity, 1000 Hertz frequency response galvanometers. Data for both cathode and anode could be obtained by reversing the direction of the applied magnetic field.

B. Experimental Results

In Figs. IV-6 and IV-7 recordings of segment currents are presented during a 0.1 sec interval of generator operation. The results given in Fig. IV-6 are typical for the segmented electrode operating as cathode, while Fig. IV-7 represents the segment currents under the same load conditions when this electrode acts as anode. Data from the electrode segment No. 6 is not shown because the corresponding instrumentation was inoperative.

The set of curves showing the time variation of the cathode currents are all different from each other indicating highly unsteady surface phenomena at the cathode. It is

apparent that during small periods of time individual segments of the cathode are carrying no current at all and that the amplitudes of current fluctuation are more than 100% of the average value. The system of curves taken from the cathode confirm the assumption of the Experimental Part IV.2.1. that most of the cathode current is carried through moving cathode spots. Because of the high velocity movement of the spots transverse to the segments it is still possible to find a representative mean value for the segment current within 0.1 sec.

In opposition to the cathode, the variations with time of the segment currents recorded from the anode all show a similar shape and are always different from zero. It is evident that there is no difference in surface phenomena for all the segments when the electrode is acting as anode. This result agrees with the fact that no electrode spots could be found on the anode surface.

In Figs. IV-8 and IV-9 recordings of segment currents for the transversely segmented electrode are shown. The results of Fig. IV-8 are typical when the electrode acts as cathode; under the same load conditions the set of curves shown in Fig. IV-9 are representative for anode operation. The set of curves obtained from the transversely segmented electrode confirm the already stated results concerning the electrical surface phenomena. Because of the movement along the individual electrode segments the current fluctuations are even more pronounced than for the axially segmented electrode.

Fig. IV-10 represents the current distribution for the transversely segmented electrode in the case of anode operation. As expected from theoretical investigations, the current distribution is symmetric about the vertical center line; but there is evidence that a considerable part of the top to bottom current is collected by the side walls. From this figure the amount of current flowing through the side walls is found to be approximately 40% of the total top-to-bottom electrode current.

The average current distributions in the flow direction, calculated from Figs. IV-6 and IV-7, are plotted in Figs. IV-11 and IV-12, respectively. Because of the special construction of segment 1, which includes the side walls, the plotted experimental value of the current through this segment has been corrected to indicate only the current which flows through the top and bottom surfaces of the electrode. This correction has been accomplished by using the results obtained from Fig. IV-10.

With the theory developed in Section II.2.2. the current density on the electrodes can be calculated from

$$j_x - ij_y = \frac{I_e}{A \frac{2\rho}{d} \cos \epsilon} \left\{ C \left[\frac{\sin \frac{\pi}{2\rho} z}{\sin \pi(c' - \frac{z}{2\rho})} \right]^{-k} + D \left[\frac{\sin \frac{\pi}{2\rho} z}{\sin \pi(c' - \frac{z}{2\rho})} \right]^{1-k} \right\}$$

where

$$C = \frac{\cos[\pi c(1-k) - \epsilon]}{\sin \pi c} \qquad D = - \frac{\cos[\pi c k + \epsilon]}{\sin \pi c} \qquad z = x + iy$$

and

$$\alpha = \tan^{-1}\Omega \quad ; \quad k = \tfrac{1}{2} - \frac{\alpha}{\pi} \qquad c' = 1 - c$$

with c as the normalized electrode length in axial direction. Included in Figs. IV-11 and IV-12 are these theoretical calculations for the cathode and anode, respectively.

IV.3. CONCLUSIONS

From the present study the following conclusions can be drawn:

1. As a main result of the experimental investigations, it could be indicated that most of the cathode current is emitted from small, regularly moving, bright cathode spots; while under the same conditions at the anode no spots at all could be detected.

2. Measuring the current distribution over the axially segmented electrode, it was found that the current distribution agrees approximately with the two-dimensional continuous theory for finitely segmented electrodes. This agreement is surprising with the presence of arc spots on the cathode.

3. The current distribution over the transversely segmented electrode is symmetric about the vertical center line of the channel. A considerable part of the electrode current is emitted or collected by the conducting side walls.
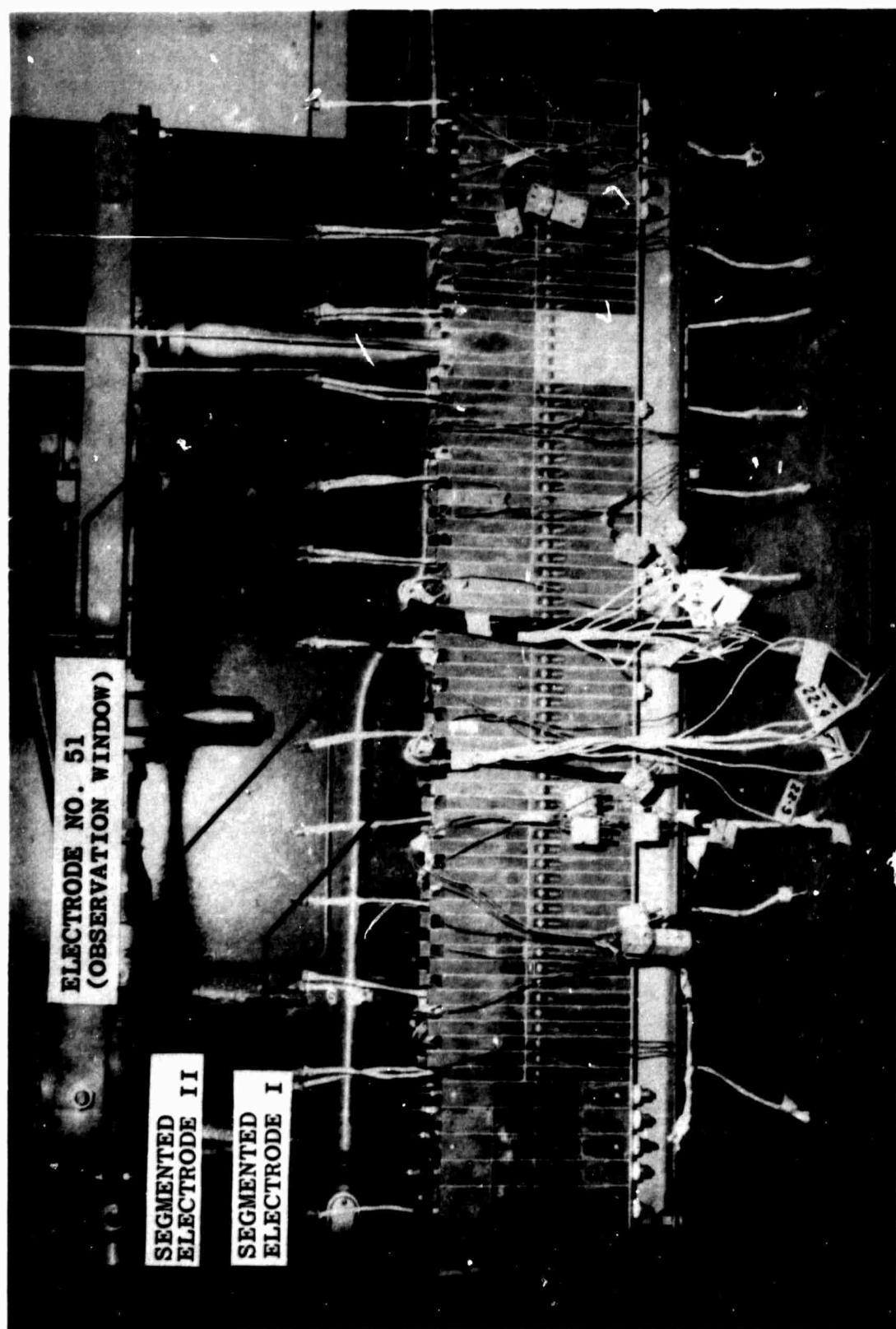
Fig. IV-1 - Location of test electrodes along Hall channel

High speed camera (view)

Observation window

Copper tube

Top part with
opening

$\overline{B}$

Gas flow

Bottom part
(photographed)

51
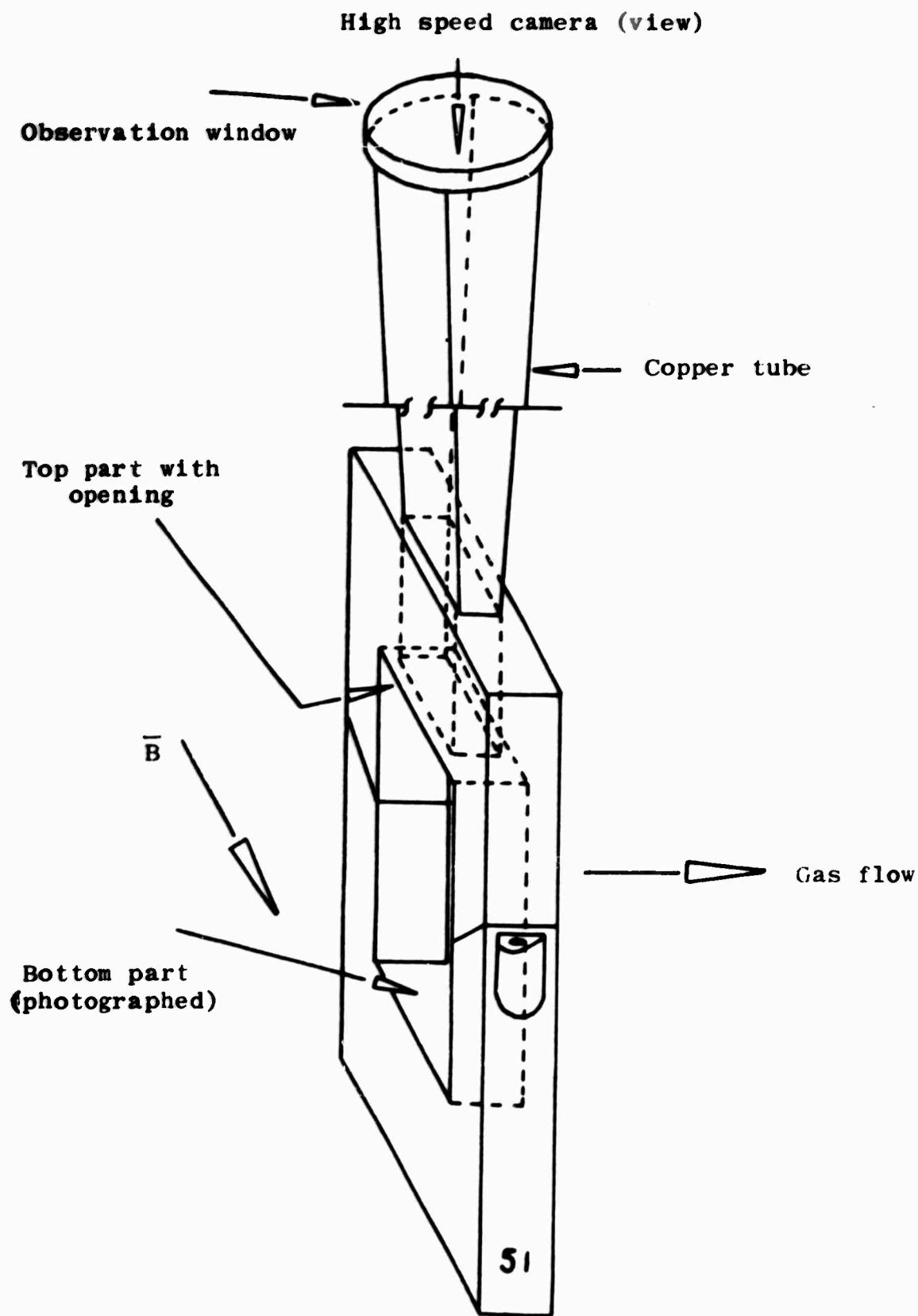
Fig. IV-2 – Schematic drawing of electrode with observation window

1.5 cm.

$\vec{v}$
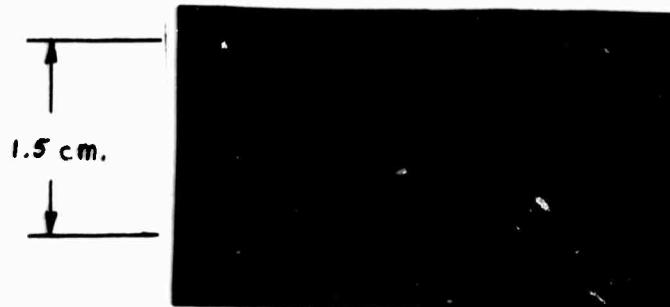
t = 0

t = .002 sec

t = .004 sec
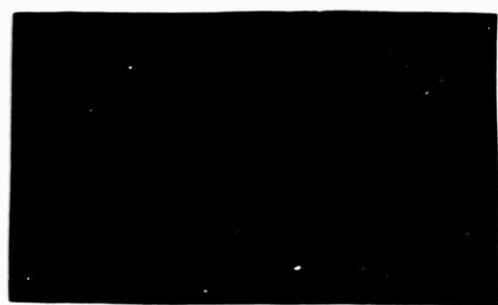
t = .006 sec

Fig. IV-3 - Electrode Spot Crossing Cathode Surface

t = .008 sec

t = .010 sec

t = .012 sec
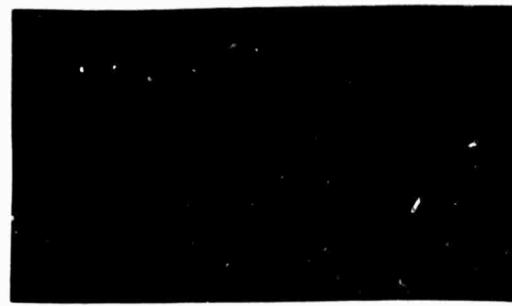
t = .014 sec

**Fig. IV-3 - (cont.).** Electrode Spot Crossing Cathode Surface
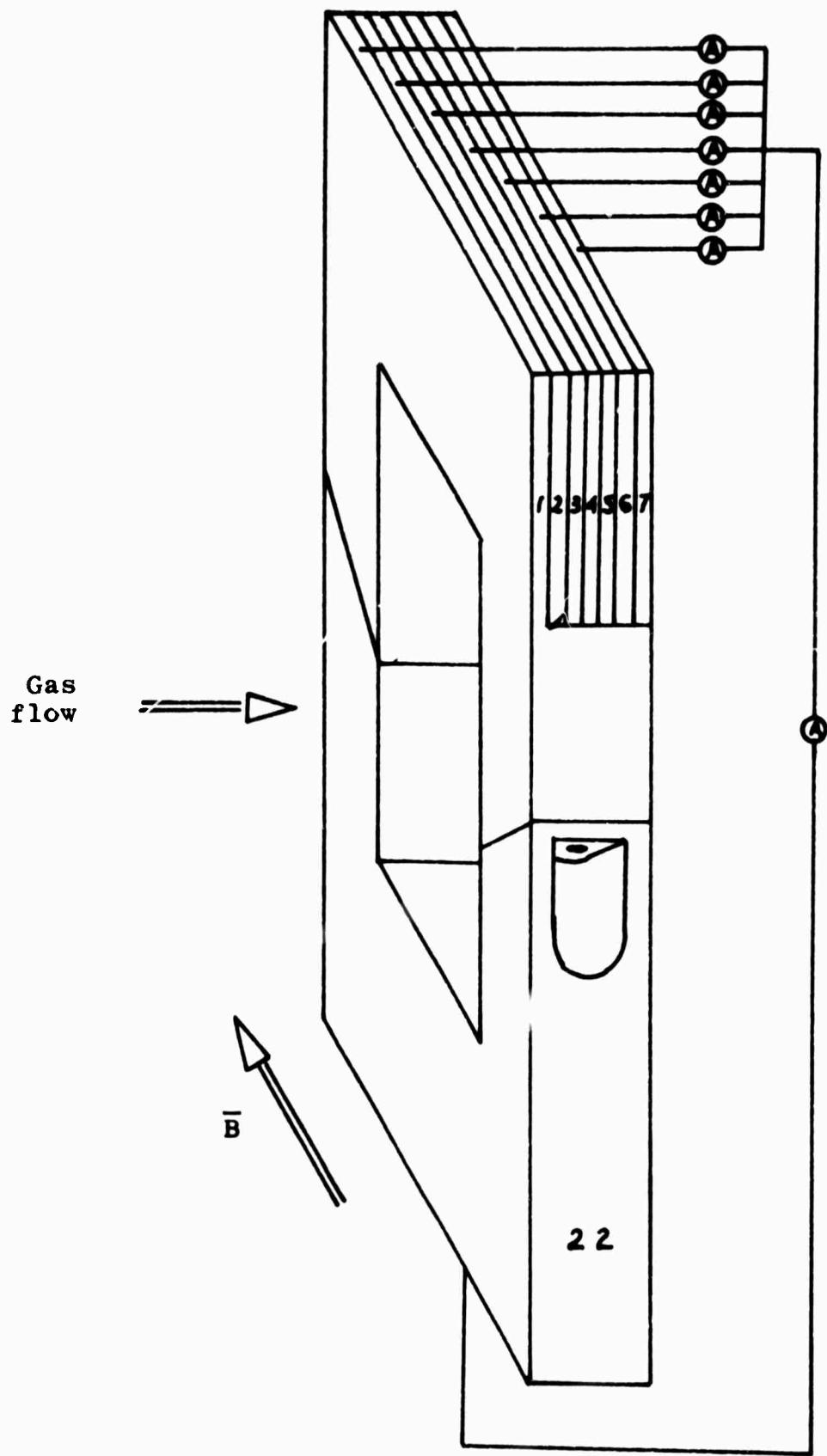
Fig. IV-4 - Schematic drawing of electrode with segmentation
parallel to the gas flow (segmented electrode I)
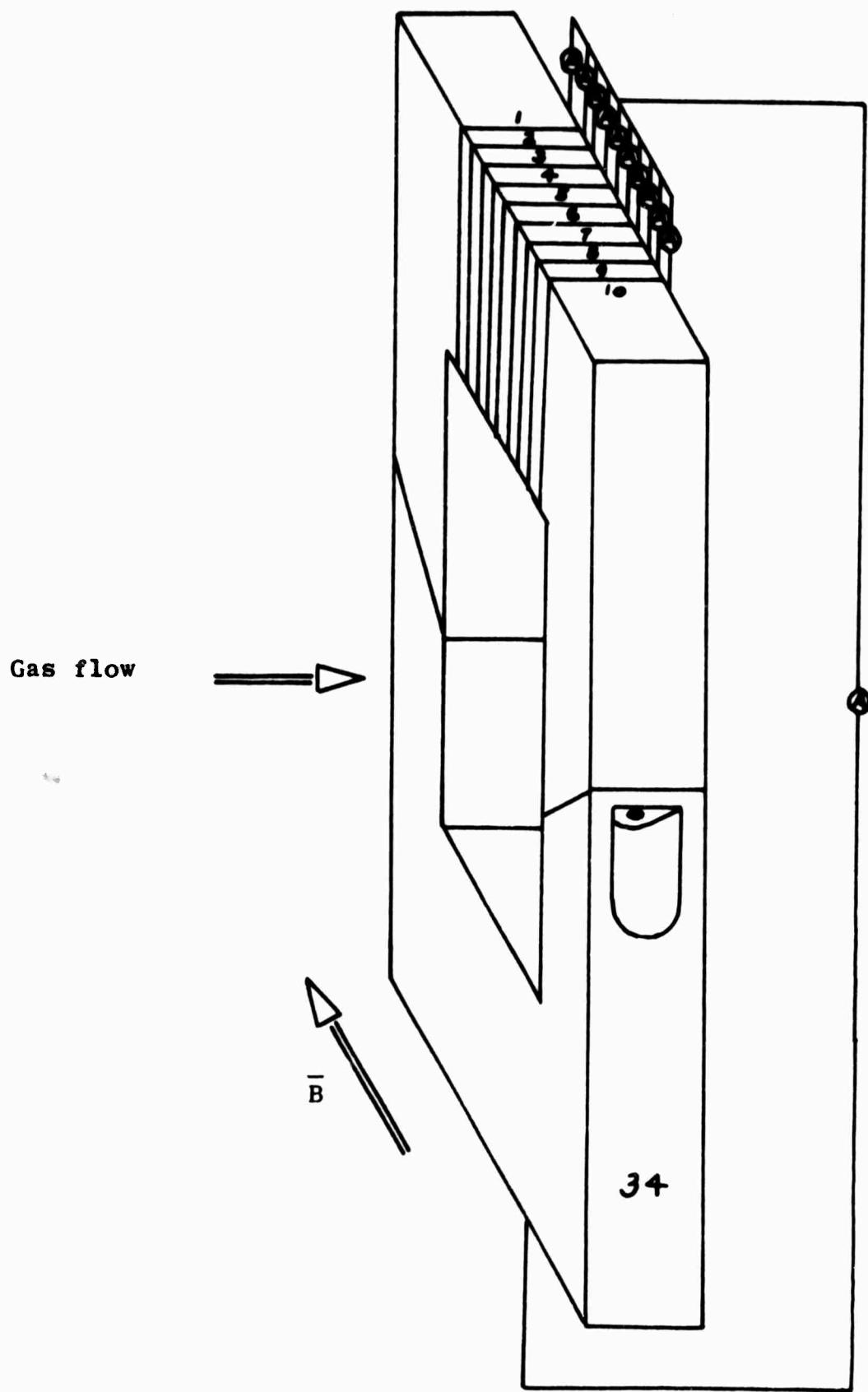
Fig. IV-5 – Schematic drawing of electrode with segmentation transverse to the gas flow (segmented electrode II)

73
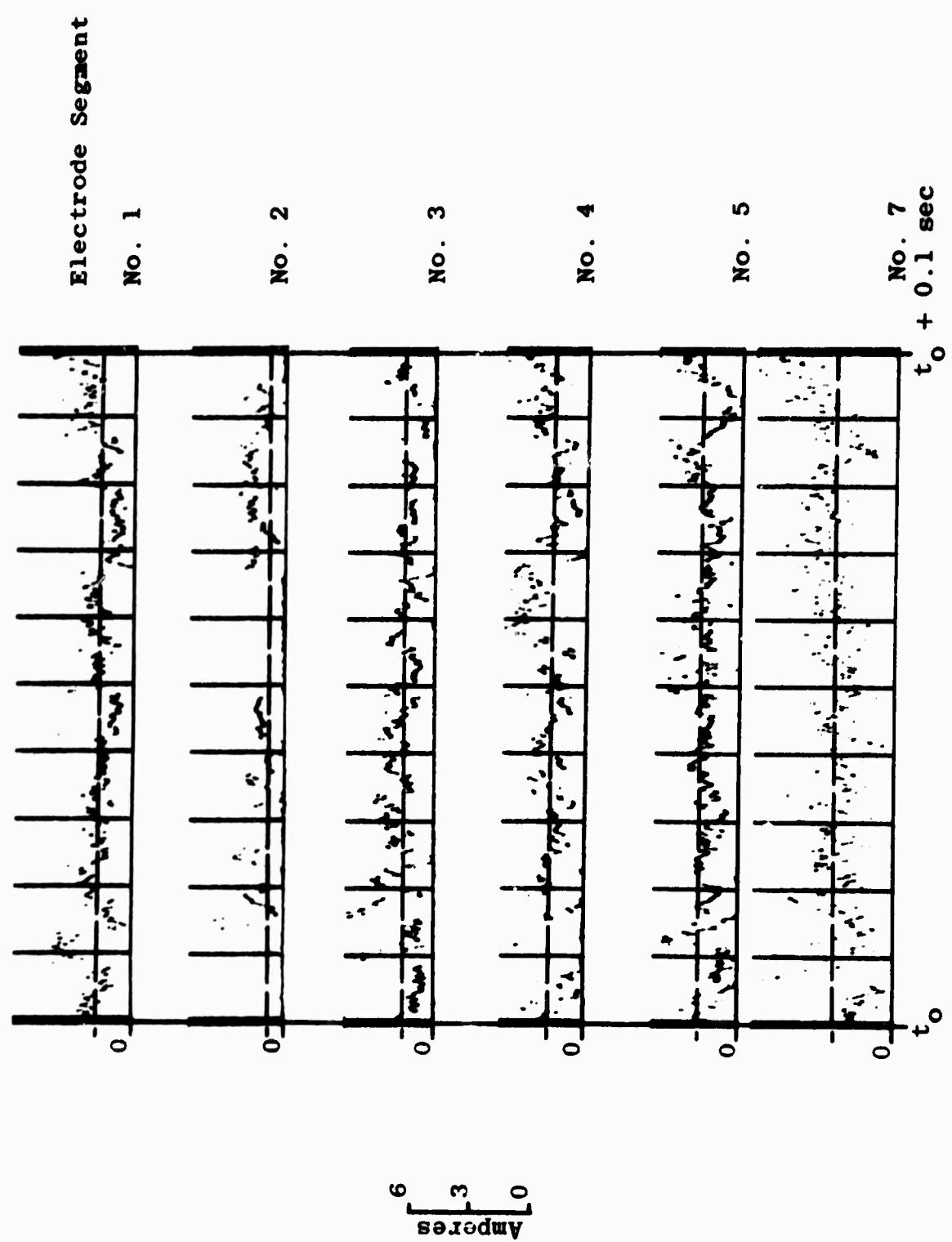
Fig. IV-6 – Time Variation of Current (Segmented Electrode I Operating as Cathode)

74
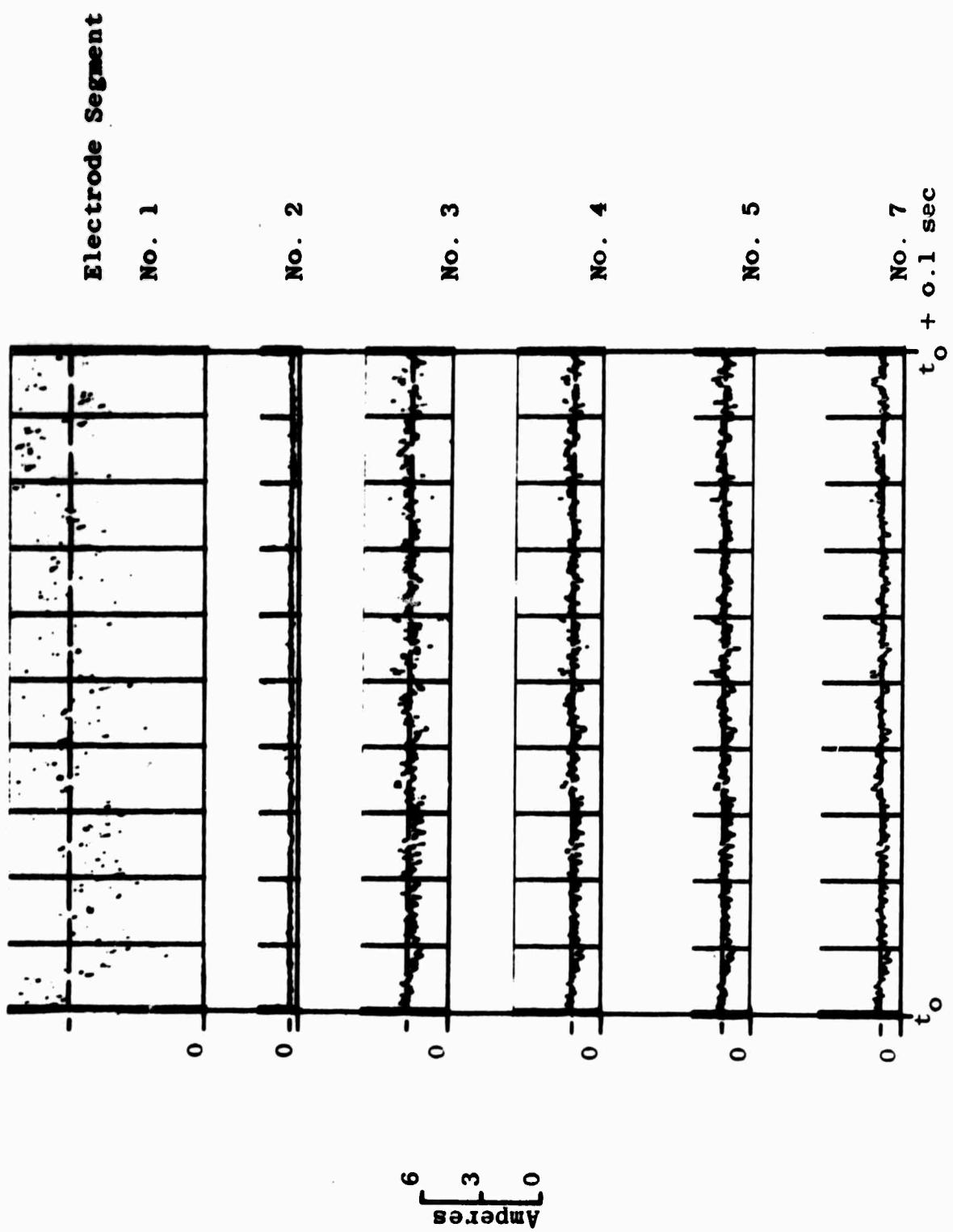
Fig. IV-7 - Time Variation of Current (Segmented Electrode I Operating as Anode)
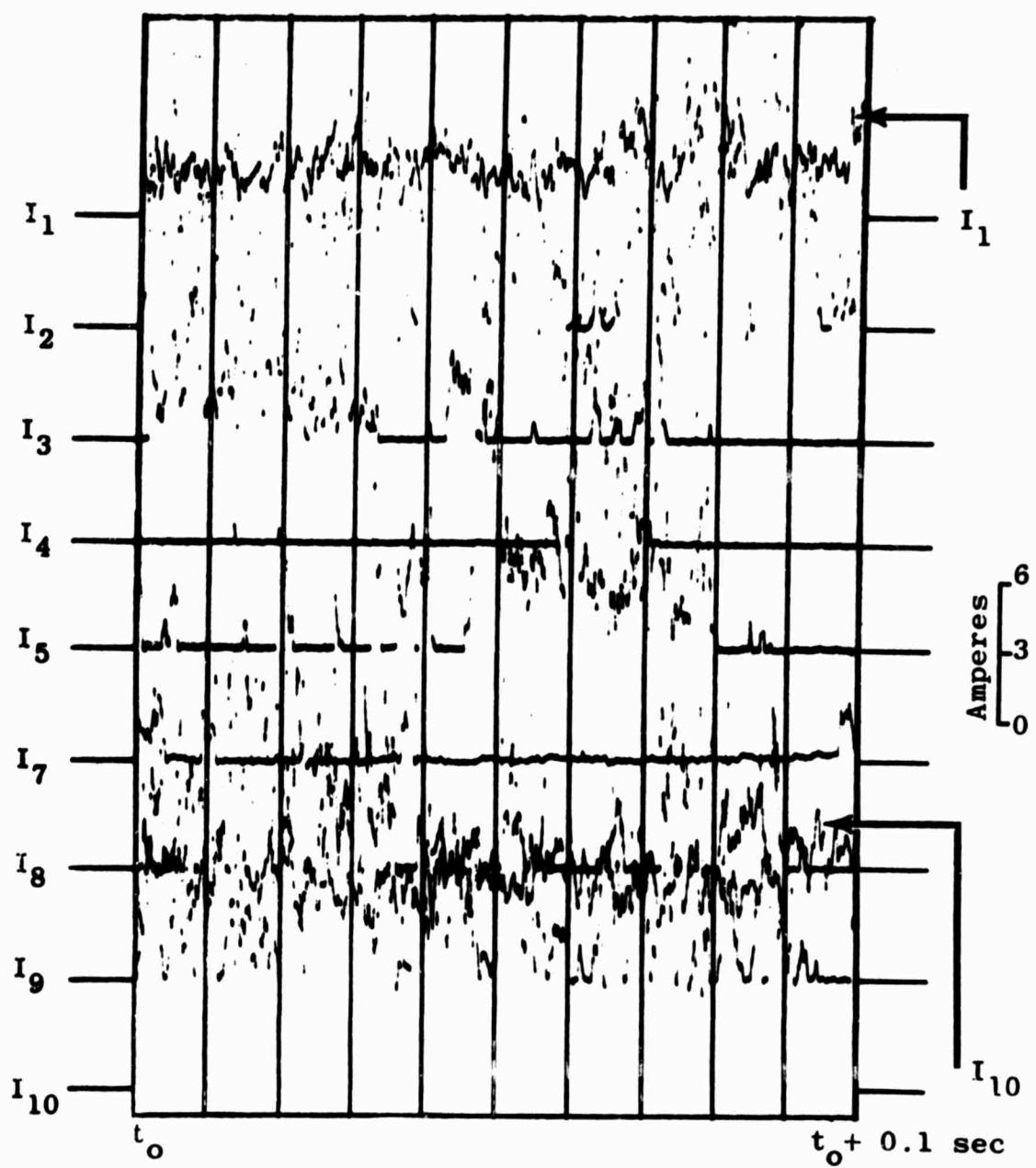
Fig. IV-8 - Time variation of current (Segmented electrode I1 operating as cathode)

Fig. IV-9 - Time variation of current (Segmented electrode II operating as anode)
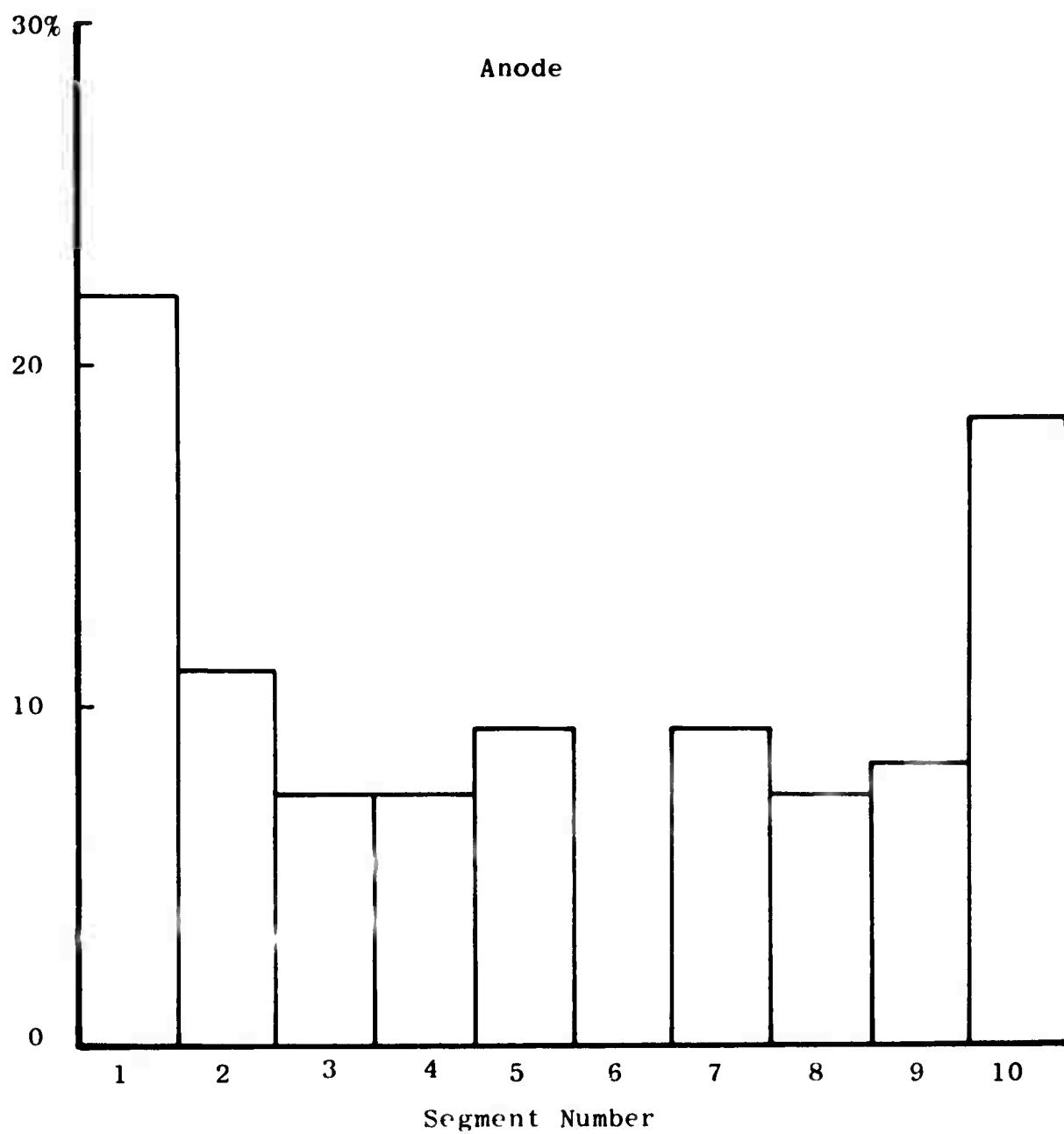
Fig. IV-10 - Current distribution over transversely segmented
electrode
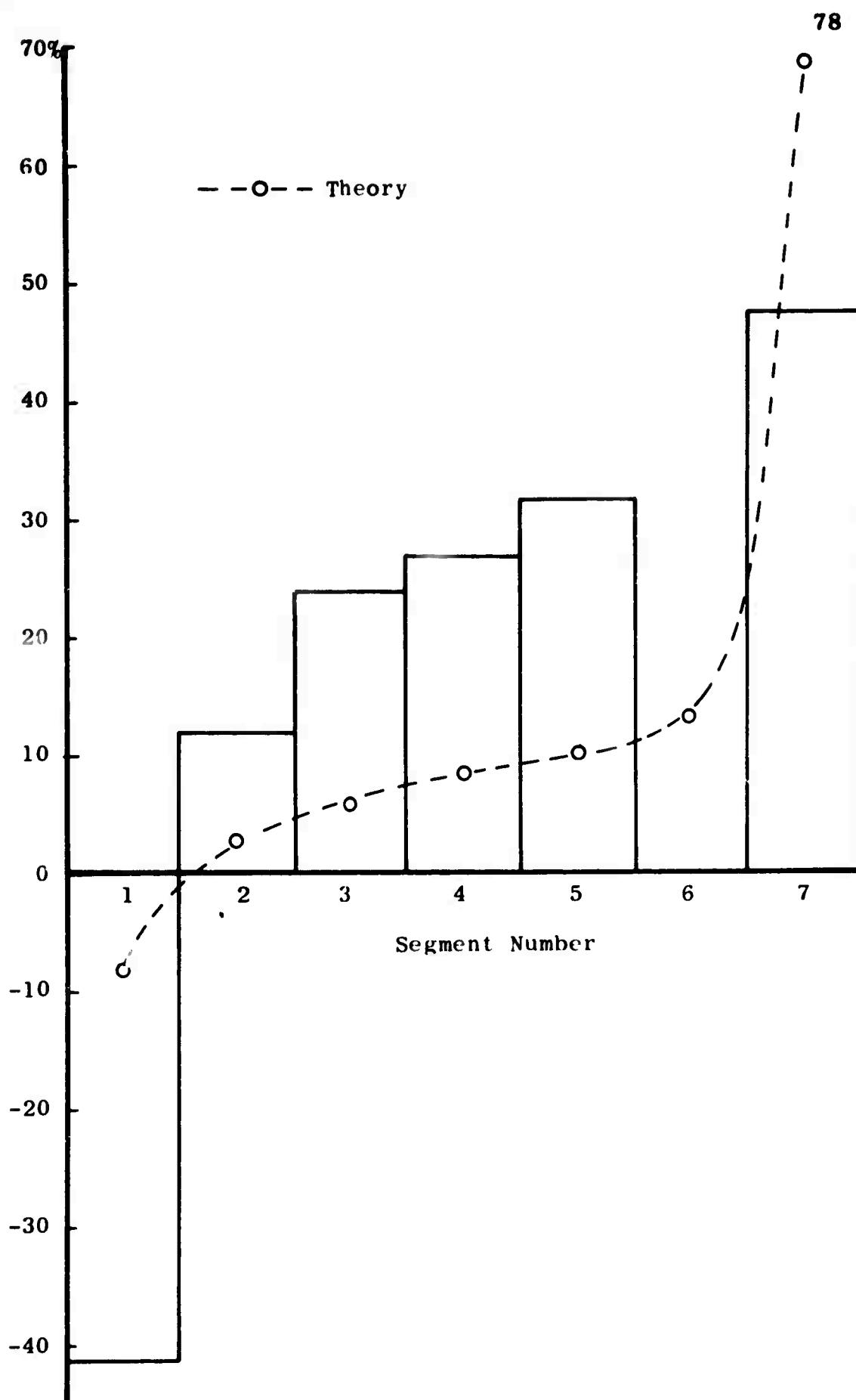
Fig. IV-11 - Current distribution over axially segmented electrode
(cathode)
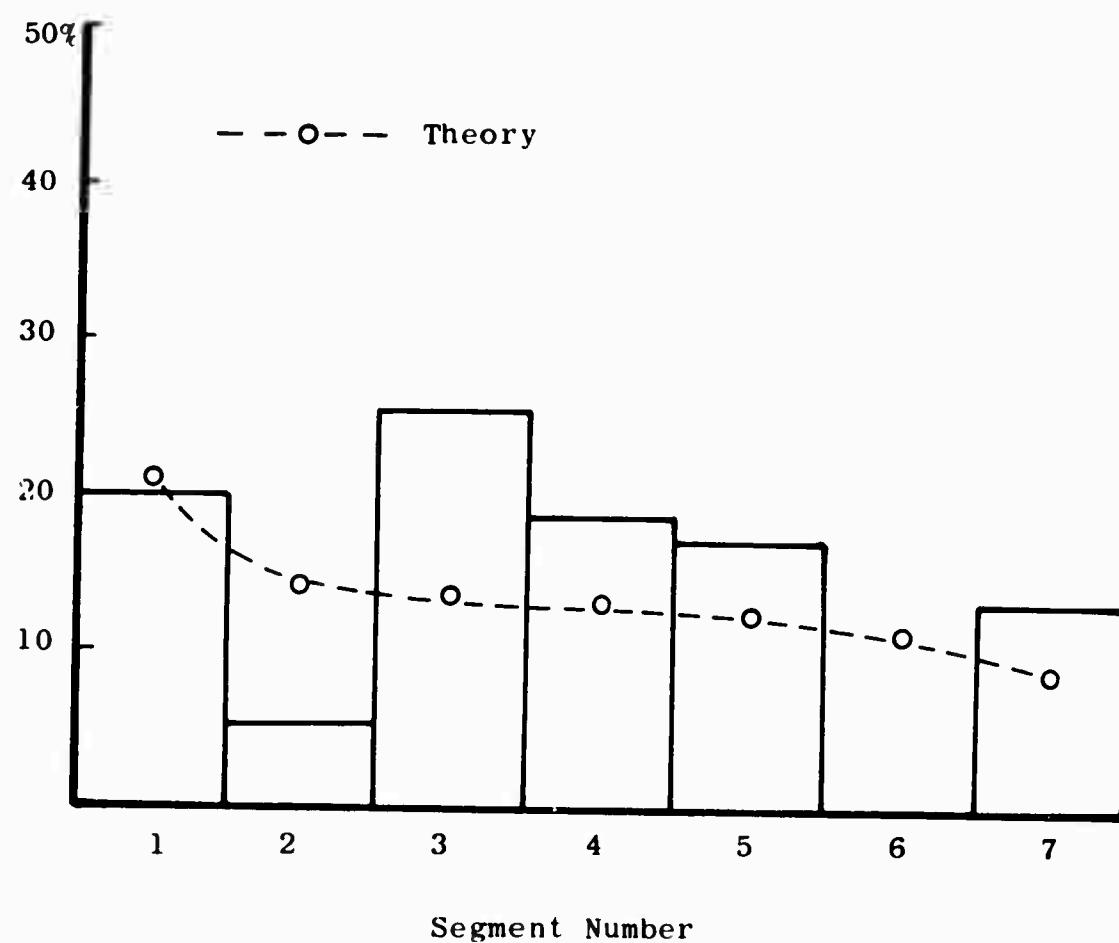
Fig. IV-12 - Current distribution over axially segmented electrode
(anode)

V. INSTABILITY STUDIES

V.1. INTRODUCTION

Preliminary investigations of the fluctuations in the Hall generator voltage were made by connecting an oscilloscope across the first 15 channel electrodes. The recordings indicated that the amplitude of these fluctuations may be as much as 100% of the average DC value. The frequency components present a range of from 250 Hz to 100 kHz. The results showed a fair degree of coherence exists between the voltage generated by a channel element at one point and that generated by one at another location. To find whether this coherence is influenced by the presence of a magnetic field, similar recordings were made in the absence of the B field but with a voltage applied across the ends of the channel. The fluctuations are considerably less in this case than with the magnetic field present, indicating that the fluctuations are enhanced by the applications of the magnetic field (Ref. V-1). In order to obtain more quantitative measurements, a more elaborate experiment has been set up; and experimental results are given here.

V.2. INSTRUMENTATION

Since the MHD generators have high DC voltages in general, isolation is needed between the generator and the recording system. A device with a wide frequency band photon-coupled isolator and a three-stage AC amplifier was designed. This instrument has a flat frequency response

within the range from 100 Hz to 120 kHz and can isolate as high as 10,000 volts DC. The device was connected across the shunt resistor from an electrode of the generator. The AC component of the electrode current was recorded on a high-speed multi-channel magnetic tape recorder simultaneously on separate channels for different electrodes (see Fig. V-1).

V.3. EXPERIMENTAL RESULTS

The experimental data were recorded from both Hall and 45° diagonal wall generators with liquid and solid fuels under different load conditions. The signals which were recorded on tape were fed into an analog computer system for power spectrum density analysis. In order to relate the experimental data with propagation velocities of the disturbances in the MHD channel, a cross-correlation function of the output signals at different electrodes of the channel is necessary. The result of this analysis is as follows. We define $\langle e_1(t) \, e_2(t + \tau) \rangle \equiv R_{12}(\tau)$ where $e_1(t)$ is the input signal to the amplifier from one station along the MHD channel at certain time t and $e_2 \, (t + \tau)$, where τ is the delay time and $R_{12}(\tau)$ is the time-averaged cross-correlation function. The cross-power spectrum density $S_{12}(\omega)$ of the input signals can be obtained from $R_{12}(\tau)$ as follows:

$$S_{12}(\omega) = \int_{-\infty}^{+\infty} R_{12}(\tau) \, \exp(-i\omega\tau)d\tau \qquad (1)$$

and the output spectrum can be related to $S_{12}(\omega)$ by

$$S'_{12}(\omega) = |\ H(\omega)\ |^2\ S_{12}(\omega)$$

Here $H(\omega)$ is the characteristic function of the isolator and amplifier; also we have

$$R'_{12}(\tau) \equiv \langle e'_{12}(t)\ e'_2(t + \tau)\rangle$$

which could be obtained experimentally. Therefore, $S'_{12}(\omega)$ could be calculated according to Eq. (1).

The total firing time was 7 seconds. Five seconds of the data for each firing were analyzed. Time-averaging techniques for random stationary signals were used. Density functions measured in terms of mean square values per unit frequency are plotted versus frequency. The noise level of the electronic analyzing system is -50 dB. In the following section, some of the results are presented.

V.3.1. Solid Fuel

In Fig. V-3, the normalized power spectrum density (PSD) for signals recorded from the Hall generator, with total generator load of 6 ohms at electrodes 47 and 51 when the instruments were connected across the top-to-bottom current meters, is shown. Maximum power density is found in the frequency range from 1000 Hz to 4000 Hz. In Fig. V-5, the results for the signals across the top-to-bottom current meter (see Fig. V-1), which were recorded from a 45° DCW generator at electrodes 39 and 43, are reported. The total generator load was 3 ohms. The frequency components for the maximum power density range are about the same as those of

the Hall generator; but the density function damps out more slowly at the high frequency end, and the signal levels are at least 5 dB higher. This may be caused by the higher overall power density generated by the 45° DCW generator.

V.3.2. Liquid Fuel

The same experiments were carried out for the liquid fuel test; unfortunately, the signals were too small to be analyzed for most of the testing data. Nevertheless, the peak power was also observed in the acoustic frequency range. One particular case is shown in Fig. V-4. The instruments were connected to electrodes 3 and 58, which are 80 cm apart, near the transition regions. The signal levels were higher due to the higher current densities at the upstream and downstream ends. The interesting fact is that the different gasdynamic properties and boundary layer thicknesses did not affect the power density spectrum.

V.3.3. Zero Magnetic Field Case

Although the oscilloscope photos showed the enhancement in fluctuations across electrodes when the B field was present, further investigations were made. The instruments were connected across three electrodes at both upstream and downstream positions, i.e., electrodes 19 and 21 and electrodes 39 and 41 (see Fig. V-2). The data were recorded during the conductivity runs without magnetic field. Total voltages of 320 volts and 200 volts DC were applied to the

total length of the MHD Hall channel with solid fuels for
firings 87 and 89, respectively. In Figs. V-6 and V-7,
the power spectrum densities are given for those two firings.
The difference observed here from the data obtained with
magnetic field is that for frequencies less than 200 Hz,
the signal amplitudes attenuate towards the downstream
end (see Figs. V-6 and V-7). This phenomenon was consistent
for three conductivity firings. Due to the complex nature
of MHD channels, a satisfactory theoretical explanation
cannot be expected at present.

V.4. CONCLUSIONS

The instability experimental results are presented in
this paper. A typical cross-correlation function is shown in
Fig. V-8; peak correlation was found at the delay time $\tau = 0$.
The zero crossing point was found at $\tau = 1.3 \times 10^{-4}$ second.
This result was obtained from a 45° DCW generator with solid
fuel. However, the cross-correlation function was not very
successfully measured. One reason is due to the fact that
these signals were recorded at stations which are close (in
the order of centimeters), and the flow velocity was on the
order of 2000 meters per second. A time resolution on the
order of microseconds is not easy to achieve by the magnetic
tape recording technique even at high speed.

Since the experimental results have been obtained,
many questions have arisen. One is the effect of spot phenom-
ena on the instability measurements. There is some indication
that this effect is small. First, the frequency of the spot

motion is lower than that measured in the instability experi-
ment. Second, some instability measurements have shown coherence
over many electrodes. Spot phenomena are not usually coherent.
Another question is whether or not the recorded fluctuations
are caused by gasdynamic fluctuations alone. If this is the
case, the presence of the magnetic field should not make any
difference in the experimental results. According to the re-
sults that have been obtained so far, this is unlikely. As
shown in Figs. V-6 and V-7, the signals recorded during the con-
ductivity test indicated that there is a spatial dependence in
the power spectrum density. In the other cases, when the mag-
netic field was applied, it appeared that there was no spatial
dependence in the PSD results. This is not fully understood
at present. Further investigations both in experiment and
theory are needed.

Although experimental results indicate fluctuations
in the channel which may be interpreted as instabilities, the
experimental conditions in an operating MHD generator are so
complex that comparison of these results with simple theory
(Ref. V-2) is not possible.

REFERENCES

V-1. Dicks, J. B., Y. C. L. Wu, S. Witkowski, R. V. Shanklin, U. Zitzow, P. Chang, and R. E. Ziemer, "Characteristics of a Family of Diagonal Conducting Wall MHD Generators," Proceedings of Eighth Symposium on Engineering Aspects of MHD, p. 46, 1967.

V-2. Powers, W. L., and J. B. Dicks, "Transient Wave Growth in Magnetogasdynamic Generators," AIAA Journal, Vol. 6, June, 1968.
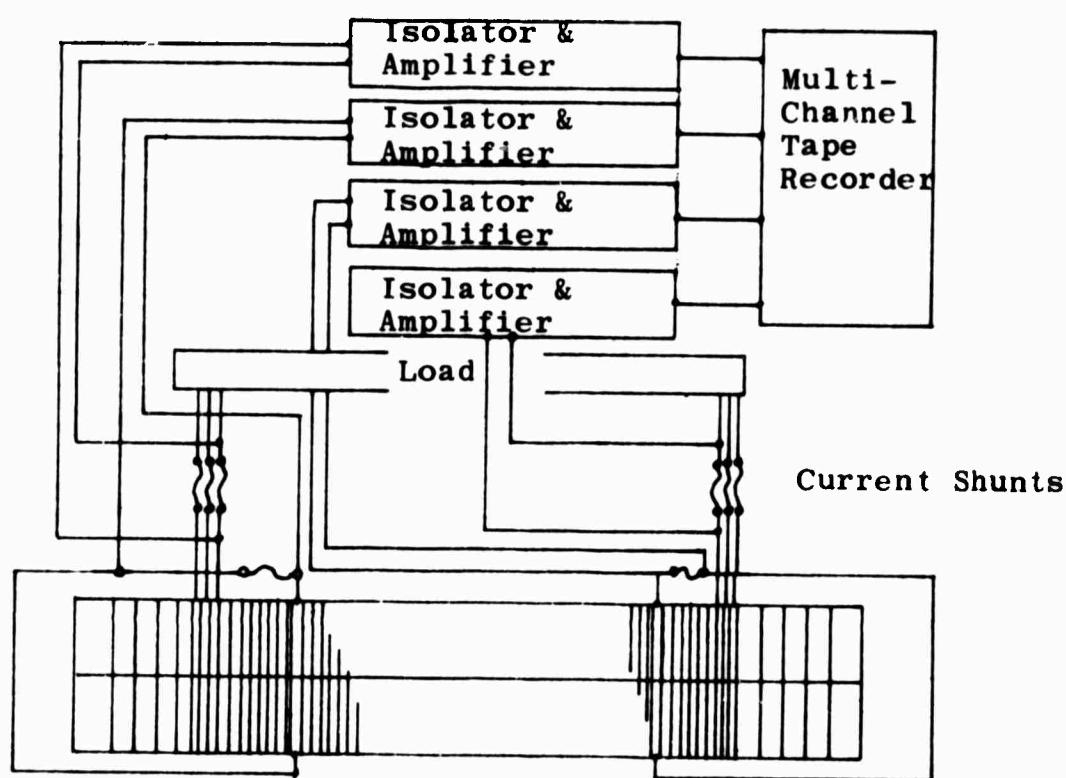
Fig. V-1 - Schematic diagram of the instruments for the insta-
bility experiment
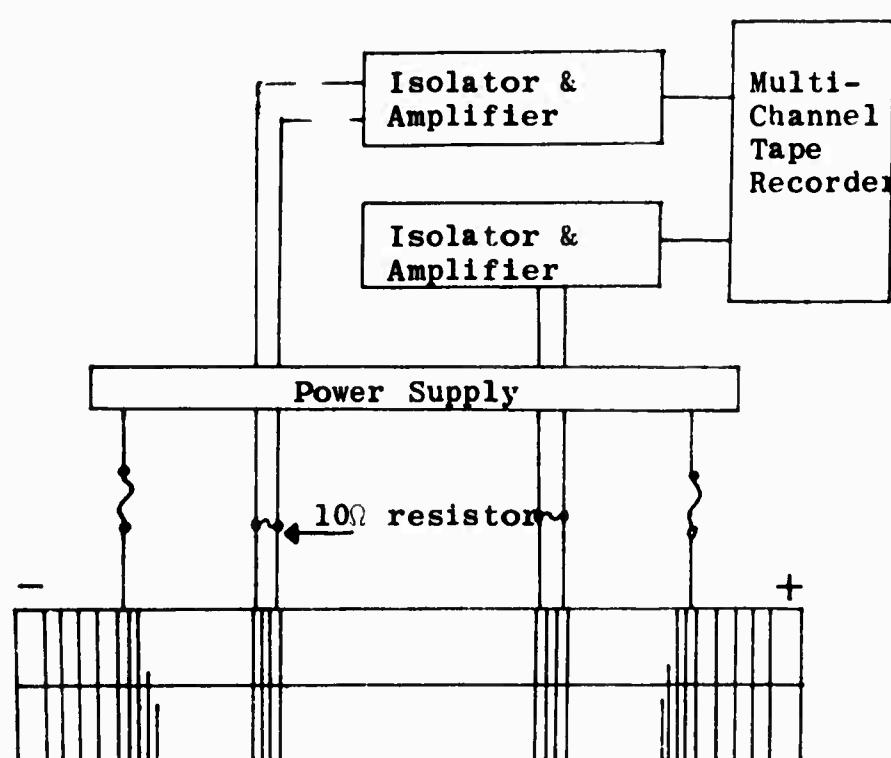
Fig. V-2 - Connections for the zero magnetic field case
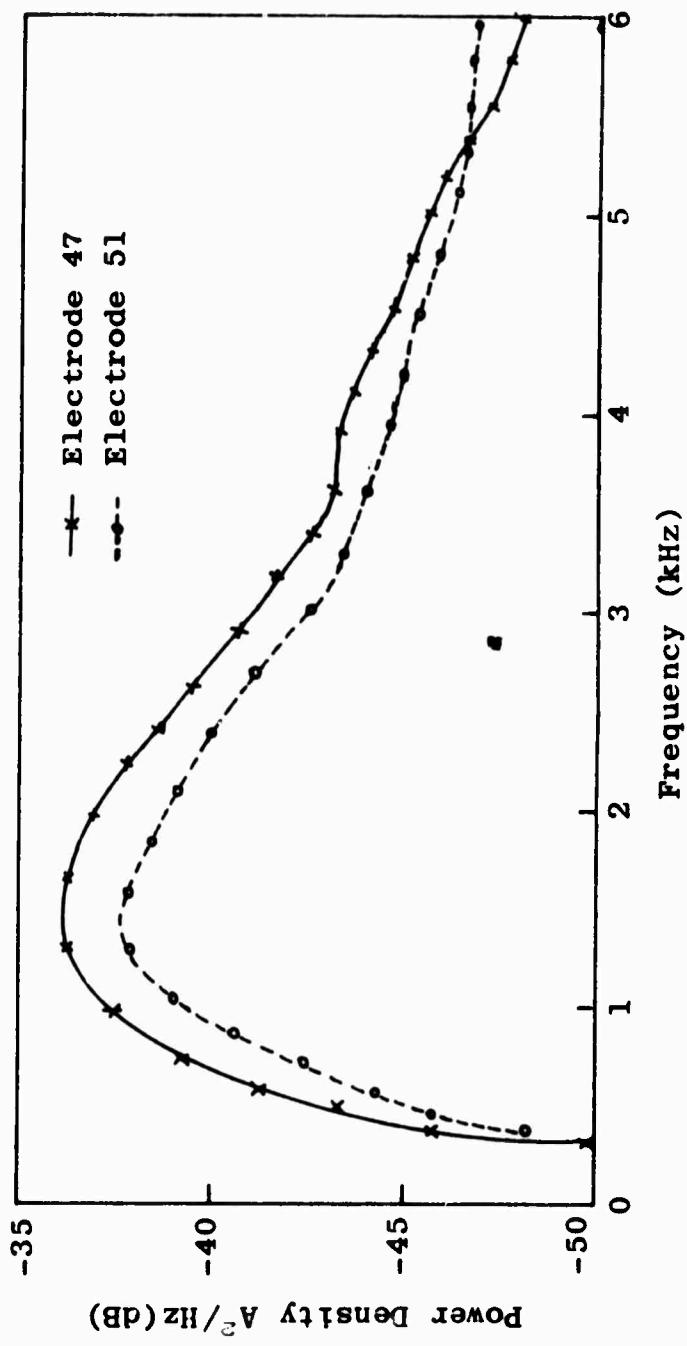
Fig. V-3 - Power spectrum density of current fluctuations in electrodes of the Hall generator
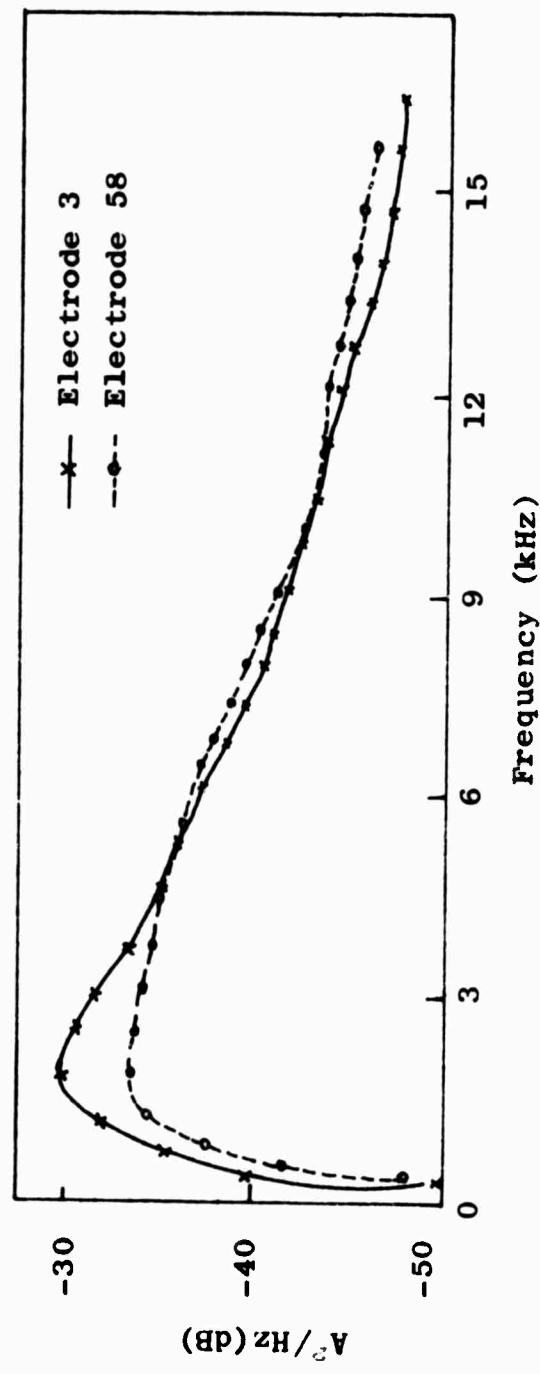
Fig. V-4 - PSD of coherent current fluctuations across the shunts connected to generator load
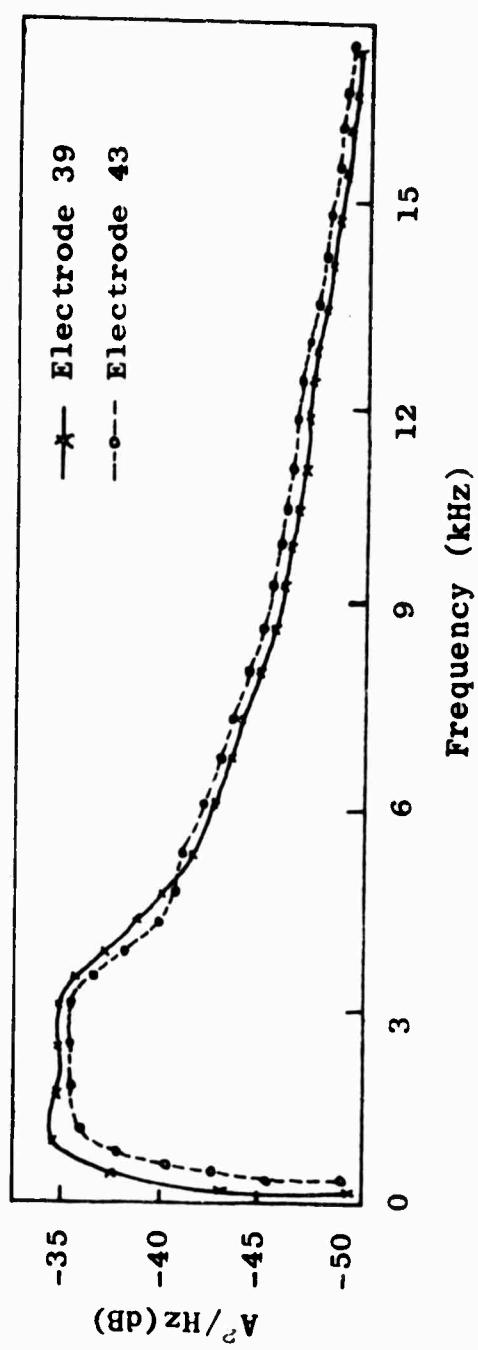
Fig. V-5 - PSD of current fluctuations in electrodes of 45° DCW generator
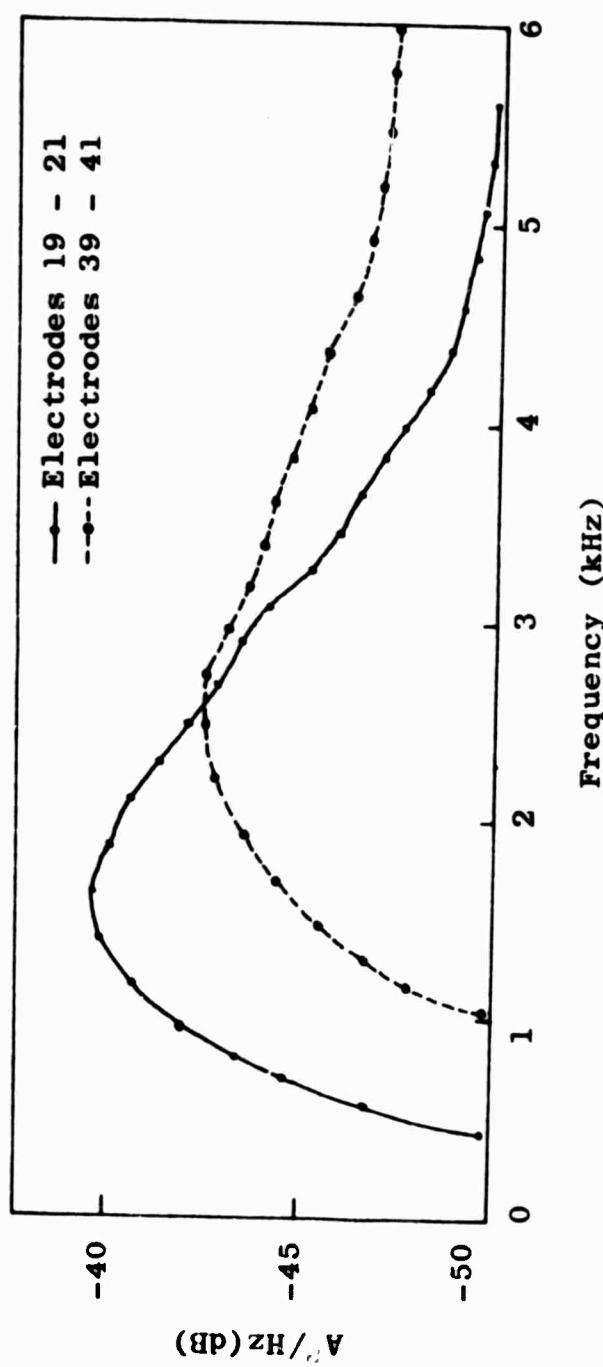
Fig. V-6 - PSD of the signals recorded from the Hall generator for zero B field case
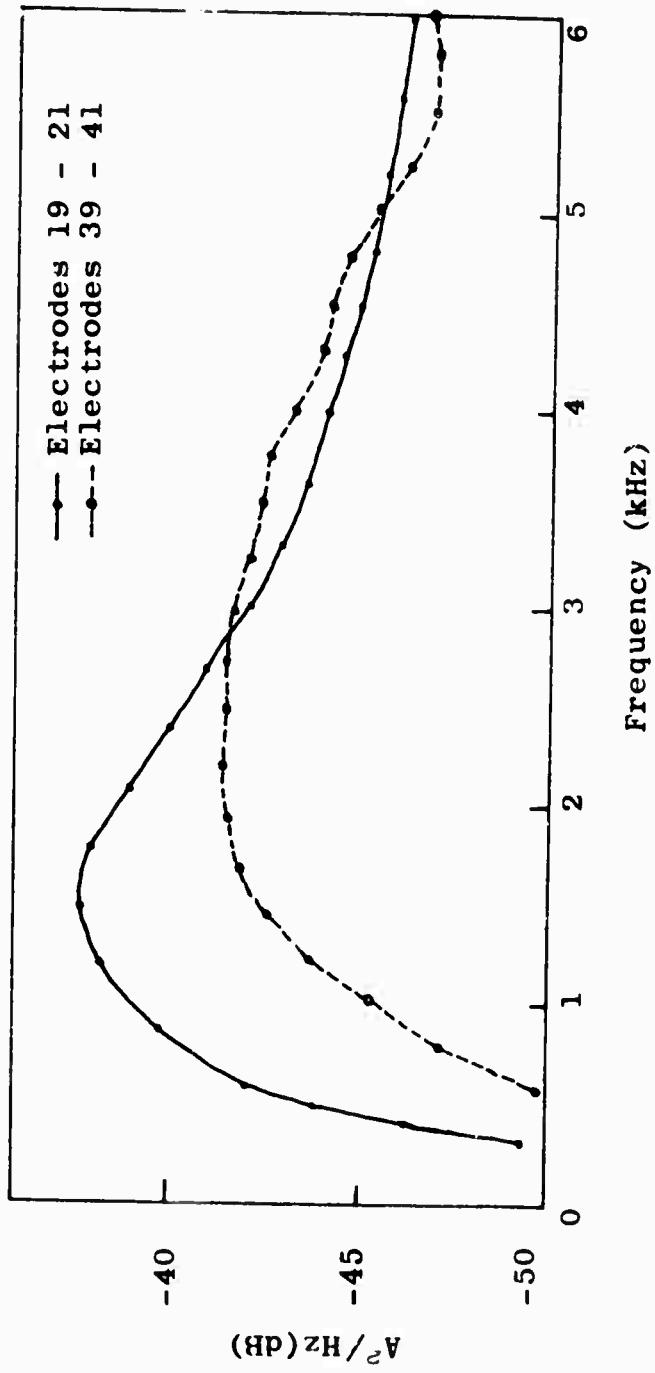
Fig. V-7 - PSD of the signals recorded from the Hall generator for zero B field case
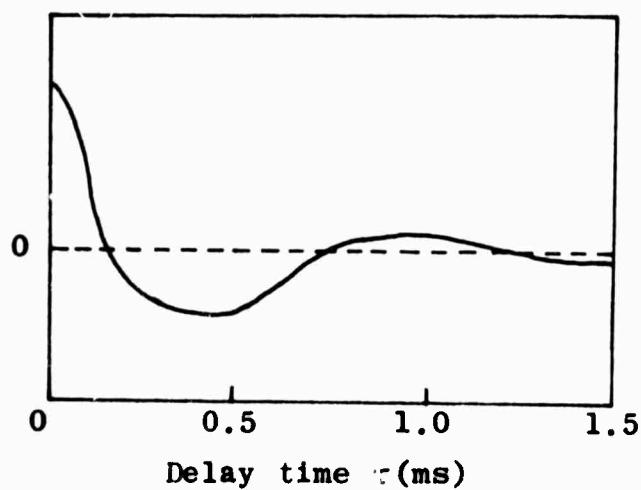
Fig. V-8 - Cross-correlation of current fluctuations over a
distance of four electrodes when the B field was
present

DOCUMENT CONTROL DATA - R & D

(Security classification of title, body of abstract and indexing annotation must be entered when the overall report is classified)

1. ORIGINATING ACTIVITY *(Corporate author)*	2a. REPORT SECURITY CLASSIFICATION
	Unclassified
The University of Tennessee Space Institute	2b. GROUP

3. REPORT TITLE

Two-Terminal Connected MHD Generators with Liquid and Solid Fuels

4. DESCRIPTIVE NOTES *(Type of report and inclusive dates)*

5. AUTHOR(S) *(First name, middle initial, last name)*

John B. Dicks, Jr., Ying-chu Lin Wu, Dieter L. Denzel, Siegbert Witkowski, Patricia Chang, J. W. Muehlhauser, Richard V. Shanklin, III, Uwe Zitzow, Robert E. Taylor and Edward S. Jett

6. REPORT DATE	7a. TOTAL NO. OF PAGES	7b. NO. OF REFS
December 1968	105	20

8a. CONTRACT OR GRANT NO. AF 33(615)-2691	9a. ORIGINATOR'S REPORT NUMBER(S)
b. PROJECT NO. 5350	AFAPL - TR - 68 - 138
c. Task No. 535004	9b. OTHER REPORT NO(S) *(Any other numbers that may be assigned this report)*
d.	

10 DISTRIBUTION STATEMENT

Distribution of this report ~~is~~

11. SUPPLEMENTARY NOTES	12. SPONSORING MILITARY ACTIVITY
	Air Force Aero Propulsion Laboratory Research and Technology Division (AFSC) Wright-Patterson AFB, Ohio 45433

13. ABSTRACT

Three DCW generators with side wall angles of 45°, 60° and 90° (Hall) of the same physical dimensions are studied. Two different types of fuels are used to drive the generator, liquid fuel consisting of RP1, gaseous oxygen and potassium hydroxide dissolved in alcohol, and double based solid fuel (manufactured and supplied by Hercules) with heavy potassium loading.

The solid fuel produced a very high conductivity (40-50 mhos/m) as compared to the liquid fuel, consequently the solid fuel generator out-performs the liquid fuel generator by a significant amount except for the Hall generator. With solid fuel the generated electrical power of a 45° DCW channel exceeded 200 KW during part of one test.

Another significant discovery of the solid fuel experiment is that the generators can run with aluminum oxide and potassium coating without large degradation in power output. Therefore, the deposit of solid particles may be used to increase generator lifetime by preventing electrode deterioration.

Now refined theoretical work is carried out to include the finite segmentation effects and current-dependent electrode drop.

DD FORM 1 NOV 65 **1473**